Atmos. Chem. Phys. Discuss., 15, 24643–24693, 2015
www.atmos-chem-phys-discuss.net/15/24643/2015/
doi:10.5194/acpd-15-24643-2015

Atmospheric Chemistry and Physics Discussions

The vertical distribution of volcanic SO_2 plumes measured by IASI

E. Carboni[1], R. G. Grainger[1], T. A. Mather[2], D. M. Pyle[2], G. Thomas[3], R. Siddans[3], A. Smith[1], A. Dudhia[1], M. L. Koukouli[4], and D. Balis[4]

[1]COMET, Atmospheric, Oceanic and Planetary Physics, University of Oxford, Clarendon Laboratory, Parks Road, Oxford OX1 3PU, UK
[2]COMET, Department of Earth Science, University of Oxford, South Park Road, Oxford OX1 3AN, UK
[3]Rutherford Appleton Laboratory, Didcot, UK
[4]Laboratory of Atmospheric Physics, Aristotle University of Thessaloniki, Thessaloniki, Greece

Received: 23 June 2015 – Accepted: 25 July 2015 – Published: 11 September 2015

Correspondence to: E. Carboni (elisa@atm.ox.ac.uk)

Published by Copernicus Publications on behalf of the European Geosciences Union.

Abstract

Sulphur dioxide (SO_2) is an important atmospheric constituent that plays a crucial role in many atmospheric processes. Volcanic eruptions are a significant source of atmospheric SO_2 and its effects and lifetime depend on the SO_2 injection altitude. The Infrared Atmospheric Sounding Instrument (IASI) on the Metop satellite can be used to study volcanic emission of SO_2 using high-spectral resolution measurements from 1000 to 1200 cm^{-1} and from 1300 to 1410 cm^{-1} (the 7.3 and 8.7 µm SO_2 bands). The scheme described in Carboni et al. (2012) has been applied to measure volcanic SO_2 amount and altitude for fourteen explosive eruptions from 2008 to 2012. The work includes a comparison with independent measurements: (i) the SO_2 column amounts from the 2010 Eyjafjallajökull plumes have been compared with Brewer ground measurements over Europe; (ii) the SO_2 plumes heights, for the 2010 Eyjafjallajökull and 2011 Grimsvötn eruptions, have been compared with CALIPSO backscatter profiles. The results of the comparisons show that IASI SO_2 measurements are not affected by underlying cloud and are consistent (within the retrieved errors) with the other measurements. The series of analysed eruptions (2008 to 2012) show that the biggest emitter of volcanic SO_2 was Nabro, followed by Kasatochi and Grímsvötn. Our observations also show a tendency for volcanic SO_2 to be injected to the level of the tropopause during many of the moderately explosive eruptions observed. For the eruptions observed, this tendency was independent of the maximum amount of SO_2 (e.g. 0.2 Tg for Dalafilla compared with 1.6 Tg for Nabro) and of the volcanic explosive index (between 3 and 5).

1 Introduction

Sulphur dioxide (SO_2) is an important atmospheric constituent, important in many atmospheric processes (Stevenson et al., 2003; Seinfeld and Pandis, 1998; Schmidt et al., 2012). Volcanic eruptions are a significant source of atmospheric SO_2, with its

ACPD
15, 24643–24693, 2015

effects and lifetime depending on the SO_2 injection altitude. In the troposphere these include acidification of rainfall, modification of cloud formation and impacts on air quality and vegetation (Ebmeier et al., 2014; Delmelle et al., 2002; Delmelle, 2003; Calabrese et al., 2011). In the stratosphere SO_2 oxidises to form a stratospheric H_2SO_4 aerosol that can affect climate for several years (Robock, 2000). Volcanoes contribute about one third of the tropospheric sulphur burden ($14 \pm 6\,Tg\,S\,yr^{-1}$; Graf et al., 1997; Textor et al., 2003). The annual amounts of volcanic SO_2 emitted is both poorly constrained and highly variable. The uncertainty in released SO_2 arises from the stochastic nature of volcanic processes, very little or no surface monitoring of many volcanoes, and from uncertainties in the contribution of volcanic sulphur emitted by quiescent (non-explosive) degassing. The effects of SO_2 in the atmosphere depend not only on the amount released but also the altitude of the plume. Altitude information is important for atmospheric chemistry, as SO_2 reactions and depletion times change with height and atmospheric composition, particularly as a function of water vapour concentration (Kroll et al., 2015; Glasow, 2010; McGonigle et al., 2004; Mather et al., 2003).

Most volcanic eruptions are accompanied by the release of SO_2 to the atmosphere, and data both on the quantity emitted, and the height at which it is injected into the atmosphere are valuable indicators of the nature of the eruption.

It is important to monitor volcanic SO_2 plumes for air safety (Brenot et al., 2014; Schmidt et al., 2014) as sulphidation of nickel alloys cause rapid degeneration of an aircraft engine (Encinas-Oropesa et al., 2008). SO_2 is also used as a proxy for the presence of volcanic ash, altough the collocation of SO_2 and ash depends upon the eruption so this approach is not always reliable for hazard avoidance (Sears et al., 2013). Mitigation strategies to avoid volcanic SO_2 and ash are currently based on ground monitoring and satellite measurements to access the location and altitude of the proximal volcanic plume, followed by the use of dispersion models to forecast the future position and concentration of the plume (Tupper and Wunderman, 2009; Bonadonna et al., 2012; Flemming and Inness, 2013). The outputs of the models are strongly dependent on the assumed initial plume altitude mainly because of the variability of the

ACPD
15, 24643–24693, 2015

wind fields with altitude. The dispersion models may use an ensemble of possible initial altitudes to identify all places where the plume can potentially arrive. Hence improving the accuracy of the initial plume altitude reduces the uncertainty in the location of the transported volcanic SO_2.

Limb viewing satellite instruments, such as the Michelson Interferometer for Passive Atmospheric Sounding (MIPAS) and the Microwave Limb Sounder (MLS), can estimate the vertical profile of SO_2 (Höpfner et al., 2013; Pumphrey et al., 2014) in the upper troposphere and lower stratosphere (UTLS), but generally cannot observe into the lower troposphere. Nadir measurements, by both spectrometers and radiometers, have been used to retrieve SO_2 column amounts, assuming the altitude of the plume, e.g., the Total Ozone Monitoring Spectrometer (TOMS, Carn et al., 2003), the Moderate Resolution Imaging Spectroradiometer (MODIS, Watson et al., 2004; Corradini et al., 2009), the Ozone Monitoring Instrument (OMI, Krotkov et al., 2006; Yang et al., 2009; Carn et al., 2009), the Atmospheric Infrared Sounder (AIRS, Prata and Bernardo, 2007), the Advanced Spaceborne Thermal Emission and Reflection Radiometer (ASTER, Pugnaghi et al., 2006; Campion et al., 2010), the Global Ozone Monitoring Experiment 2 (GOME-2, Rix et al., 2012), and the Spinning Enhanced Visible and Infrared Imager (SEVIRI, Prata and Kerkmann, 2007).

Nadir spectrometer measurements in the ultraviolet (OMI, GOME-2) and infrared (AIRS, the Tropospheric Emission Sounder, TES, IASI) can be used to infer information on the SO_2 plume altitude. This is based on the fact that the top-of-atmosphere radiance of a plume, with the same amount of SO_2 but at another altitude, will have a different spectral shape within the SO_2 absorption bands.

UV spectra have been used to retrieve information on SO_2 altitude by Nowlan et al. (2011) using an optimal estimation retrieval applied to GOME-2 measurements. Yang et al. (2010) used a direct fitting algorithm to retrieve the SO_2 amount and altitude from OMI data. Both of these techniques were applied to the 2008 Kasatochi eruption which injected a relatively large amount of SO_2 high (circa 12 km) in the atmosphere.

ACPD
15, 24643–24693, 2015

A new scheme to retrieve altitude from GOME-2 has been developed by Van Gent et al. (2015) and applied to Icelandic eruption case studies (Koukouli et al., 2014).

Volcanic SO_2 retrievals from satellite data in the thermal infra-red (TIR) part of the spectrum are based on two regions of SO_2 absorption around 7.3 and 8.7 µm. The strongest SO_2 band is at 7.3 µm. This is in a strong water vapour (H_2O) absorption band and is not very sensitive to emission from the surface and lower atmosphere. Above the lower atmosphere this band contains information on the vertical profile of SO_2. Fortunately differences between the H_2O and SO_2 emission spectra allow the signals from the two gases to be decoupled in high resolution measurements. The 8.7 µm absorption feature is in an atmospheric window so it contains information on SO_2 from throughout the column. In Clerbaux et al. (2008) the SO_2 absorbing feature around 8.7 µm was used to retrieve the total SO_2 amount and profile from TES data by exploiting this instruments ability to resolve the change in SO_2 line-width with pressure. The 7.3 µm spectral range has been used by Clarisse et al. (2014) in a fast retrieval of SO_2 altitude and amount. Their approach, based on Walker et al. (2012), assumes that the SO_2 is located at different altitudes, choosing the altitude that gives the best spectral fit.

In this paper, the Carboni et al. (2012) retrieval scheme (hereafter C12) has been applied to study the vertical distribution of SO_2 for the major eruptions during the period 2008–2012 and for some minor low tropospheric eruptions such as an Etna lava fountain.

The aims of this paper are to test the retreived SO_2 amount and altitude against other datasets (we used CALIPSO backscattering profile to test the altitudes and Brewer ground measurements for the column amounts) and to study the volcanic plumes from different eruption types and in different locations.

ACPD
15, 24643–24693, 2015

2 IASI data

There are currently IASI sensors on-board the European weather satellites METOP-A and METOP-B. METOP-A has been operating since 2007 and was the first of three satellites scheduled to operate for a total of 14 years. METOP-B has been operating since September 2012. The satellites cross the Equator on the descending node at a local time of around 9:30 a.m.

IASI is a Fourier transform spectrometer covering the spectral range 645–2760 cm^{-1} (3.62 to 15.5 µm) with spectral sampling of 0.25 cm^{-1} and an apodized spectral resolution of 0.5 cm^{-1} (Blumstein et al., 2004). It has a nominal radiometric noise (NeDT at 280 K) of 0.1–0.2 K (650–1750 cm^{-1}). The field-of-view (FOV) consists of four circular footprints of 12 km diameter (at nadir) inside a square of 50 km × 50 km, step-scanned across track (with 30 steps). The swath is 2100 km wide and the instrument can nominally achieve global coverage in twelve hours.

Observations are co-located with the Advanced Very High Resolution Radiometer (AVHRR), providing complementary visible/near infrared measurements. IASI carries out nadir observation of the Earth simultaneously with the Global Ozone Monitoring Experiment (GOME-2) also on-board METOP. GOME-2 is a UV spectrometer measuring SO_2 in the UV absorption band and is used for both Differential Optical Absorption Spectroscopy (DOAS) (Rix et al., 2012) and optimal estimation retrievals (Nowlan et al., 2011) of SO_2. More information about IASI can be found in Clerbaux et al. (2009). The IASI level 1 C data (geolocated with apodized spectra) used here were obtained from both the British Atmospheric Data Centre (BADC) archive and EUMETSAT Unified Meteorological Archive Facility (UMARF) archive.

3 SO_2 retrieval scheme

The retrieval scheme follows Carboni et al. (2012) where the SO_2 concentration is parametrised as a Gaussian profile in pressure (with 100 mb spread). Using IASI mea-

ACPD
15, 24643–24693, 2015

surements from 1000 to 1200 cm^{-1} and from 1300 to 1410 cm^{-1}, an optimal estimation retrieval (Rodgers, 2000) is employed to estimate the SO_2 column amount, the height and spread of the SO_2 profile, and the surface skin temperature.

The forward model, based on Radiative Transfer model for TOVS (RTTOV) (Saunders et al., 1999) but extended to include SO_2 explicitly, uses ECMWF temperatures interpolated to the measurement time and location. The retrieval technique uses an error covariance matrix, based on a climatology of differences between the IASI measurements and SO_2-free forward modelled spectra. Any differences not related to SO_2 between IASI spectra and those simulated by a forward model are included in the covariance matrix. Note that the SO_2 retrieval is not affected by underlying cloud. If the SO_2 is within or below an ash or cloud layer its signal will be masked and the retrieval will underestimate the SO_2 amount, in the case of ash this is indicated by a cost function value greater than two.

The retrieval is performed for every pixel where the SO_2 detection result is positive (Walker et al., 2011, 2012). The scheme iteratively fits the forward model (simulations) with the measurements, to seek a minimum of a cost function. The solution, when the measurements do not contain enough information to retrieve all the parameters in the state vector, is strongly affected by the assumed a priori values. When the SO_2 amount decreases, the spectral information decreases, and is it not possible to retrieve both SO_2 amount and altitude. This often happens at the edge of the plume. In this work we use 400 ± 500 mb as the a priori value for plume altitude and 0.5 ± 100 DU for column amount. In addition, only quality controlled pixels are considered; these are values where the minimisation routine converges within 10 iterations, the SO_2 amount is positive, the plume pressure is below 1000 mb and the cost function is less then 10.

Rigorous error propagation, including the incorporation of forward model and forward model parameter error, is built into the system, providing quality control and error estimates on the retrieved state. Retrieved uncertainties increase with decreasing altitude, nevertheless it is possible to retrieve information in the lower troposphere and monitor volcanic degassing. In the case of two or multiple SO_2 layers the forward model as-

ACPD
15, 24643–24693, 2015

sumption of a single Gaussian layer is a source of error (and this error is not included in the pixel by pixel error estimate). In this case the retrieved altitude is an effective altitude between the two (or more) plume layers; in particular the altitude will be the one that is radiatively closer to the measured spectra and the altitude will be the radiatively equivalent altitude.

The altitude of the SO_2 plume strongly modulates the retrieval error as the contrast between plume temperature and surface temperature is a critical factor. The error in SO_2 amount decreases with an increase in plume altitude. Typical uncertainties are 2 DU for a plume centred at 1.5 km and less then 1 DU for plumes above 3 km.

When using the result from this setting of the retrieval scheme the following caveats should be considered:

1. The retrieval is valid for SO_2 column amounts less then 100 DU (limit used in the computation of RTTOV coefficients) and altitudes less then 20 km (due to the used Gaussian profile with 100 mb spread). For higher eruptions one should use a thinner Gaussian profile, for column amounts bigger then 100 DU new RTTOV coefficients will be needed. At present both of these conditions produce results that do not pass the quality control.

2. Quality control and orbit gaps can produce artefacts (see Sect. 6).

3. Care should be taken when using the altitude to infer if a plume is above or below the tropopause. In this case, it is desirable to combine or confirm these measurements using other measurements. This is because there are altitudes with the same temperature above and below the tropopause, and the SO_2 signal could be similar. Nevertheless, the IASI spectrum contains altitude information from the overlapping of SO_2 with other gas absorption.

4. The global annual mean variability between real atmospheric profiles and ECMWF profiles is included in the error covariance matrix, and then propagated into the retrieval errors. However we cannot exclude some extreme events where

ACPD
15, 24643–24693, 2015

the difference between ECMWF profiles and the real profile is at the tail of the annual global statistical distribution. In this case, local and seasonal covariance matrices could be used. For the retrievals presented here a global covariance matrix has been used, computed using days from all four seasons.

5. Volcanoes also emit water vapour. If this emission is larger than the water vapour variability considered in the error covariance matrix, the results could be affected by errors that are not included in the output errors.

4 Altitude comparison with CALIOP

Vertical profiles of aerosol and clouds are provided by NASA's Cloud Aerosol Lidar with Orthogonal Polarization instrument (CALIOP, Winker et al., 2009) carried on the CALIPSO satellite. CALIOP's vertical/horizontal resolution is 0.06/1.0 km at altitudes between 8.2 and 20.2 km. CALIPSO is part of the A-train with an equatorial overpass time of ∼ 13.30. CALIOP and IASI have coincident measurements around ±70° latitude and moving from this latitude towards the equator causes the time difference between the two measurements to increase.

CALIOP backscatter profile have been averaged (to 3 km along-track, 250 m vertical) and CALIOP observations of volcanic plumes have been identified using SEVIRI false colour images based on the infrared channel at 8.7, 11 and 12 µm (Thomas and Siddans, 2015).

The criteria used to define a coincidence between CALIOP and IASI pixels were: a distance of < 100 km and a time difference of < 2 h. With these relatively strict criteria, the selected coincident data are only from the Icelandic Eyjafallajökull and Grimsvötn eruptions. For the other eruptions considered (Puyehue-Cordón Caulle, June 2011; Nabro, June 2011; Soufrière Hills, February 2010) the differences in acquisition time between the CALIOP and IASI measurements are more than 2 h. It may be possible to

ACPD
15, 24643–24693, 2015

analyse these eruptions in the future by using the wind field to account for the movement of the plume with time.

Figure 1 shows the comparison between CALIOP and IASI for the Eyjafjallajökull plume on the 7 May 2010. This is the CALIOP track presented by Thomas and Prata (2011) in which they identify both ash and SO_2 plumes in the southern part of the track (less then 55° N) and SO_2 only plumes in the northern part of the track (the scattering feature around 5 km between 55–60° N where the scattering signal is possibly from H_2SO_4 aerosol resulting from the oxidation of volcanic SO_2).

Ash and SO_2 are not necessarily advected together (Thomas and Prata, 2011; Sears et al., 2013), but in these case studies (Figs. 1–4), there is good agreement between IASI and the backscattering features within the IASI error bars. This may be due to the presence of H_2SO_4 associated with the SO_2 plume. An important aspect to note is that in nearly all of the coincidences for the Eyjafallajökull case (with the exception of a few pixels on 14 May) the volcanic plume is above a lower meteorological cloud. This is identifiable as the scattering layer at around 1 km height in Fig. 1 and between 1 and 4 km in Figs. 2 and 3. This comparison against CALIOP in the presence of water cloud confirms that the retrieval is not affected by underlying cloud. This is because the variability that such cloud introduces is represented by the error covariance matrix which includes radiance differences between the clear forward model and cloudy IASI spectra. An accurate retrieval of altitude is also an important factor for the estimate of SO_2 amount, this is because the thermal SO_2 signal can be up to one order of magnitude different between different altitudes. A good comparison of altitude with CALIPSO then gives confidence in both altitude and column amount.

Figure 4 shows the Grimsvötn plume at the beginning of the eruption. There is separation between the higher part of the plume (dominated by SO_2) moving higher and spreading north, and the lower part of the plume (dominated by ash, but still with some SO_2 associated with it) moving south-west. It was this part of the plume that moved over Europe in the following days and caused airspace closure.

ACPD
15, 24643–24693, 2015

5 Comparison with Brewer ground data

During the Eyjafjallajökull eruption in April and May 2010, the volcanic plume overpassed several European ground measurement stations equipped with Brewer instruments. Brewer instruments are UV spectrophotometers, principally dedicated to measuring the total ozone column but also capable of determining total column SO_2 (Kerr et al., 1981). Extraction of the SO_2 signal from the UV measurements is performed as a second step after the ozone quantity retrieval due to the much lower SO_2 absorption features strength (De Muer and De Backer, 1992). Depending on the amount of atmospheric SO_2 affecting the instruments, the Brewer spectrophotometer has been shown to be sensitive both to anthropogenic SO_2 loading in the lower troposphere (Zerefos et al., 2000) as well as to an overpass of a volcanic plume, which produces a strong SO_2 signal within the ozone absorption bands. These ground-based measurements have lately been used in Rix et al. (2012) in a comparison with the GOME-2/Metop-A SO_2 retrievals and in the validation work of the European Space Agency, ESA, projects (SMASH and SACS2[1]) on the 2010 and 2011 Icelandic eruptions (Koukouli et al., 2014). The World Ozone and Ultraviolet Radiation Data Centre (WOUDC) is an active archive facility that includes quality-assured Brewer ground-based O_3 measurements and also provides SO_2 daily averages. The dataset for April and May 2010 was downloaded from the WOUDC archive (http://www.woudc.org/) for all European sites with Brewer instruments.

The reported SO_2 amount in non-volcanic conditions (e.g. over Europe before 15 April 2010) from Brewer stations varies considerably which can mostly be attributed to the small signal-to-noise ratio of the SO_2 signal compared to the ozone signal. This variability may also be due to insufficient reported data quality control with respect to SO_2 retrieval, since most stations focus on the quality of the ozone measurements and not their by-products. Negative values can also be present in the daily average

[1] "Study on an End-to-End system for volcanic ash plume monitoring and prediction" (SMASH) and "Support to aviation control service 2" (SMASH2).

ACPD
15, 24643–24693, 2015

datasets, a result of the nominal Brewer algorithm's inability to resolve small atmospheric SO_2 amounts. Therefore, only a subset of the available Brewer sites in the WOUDC database were selected for this study. Stations were not selected if they reported a majority of negative values (such as Reading, UK; La Coruna, Spain, and so on) for the two months considered (April and May 2010), or had negative values less than −1 DU (such as Madrid, Spain; Poprad-Ganovce, Slovakia). These negative values point to the small amount of the volcanic gas reaching the specific locations. Despite recording several negative values, the Valencia, Spain, site was considered since it was presented in Rix et al. (2012), after checking that the measurements coincident with the presence of the IASI plume were statistically significantly larger than the average background measurements.

All the positive values of the selected ground stations (listed in Fig. 5) have been compared with the IASI measurements of the SO_2 plume. The SO_2 estimates available from WOUDC are daily averages. In order to compare these datasets with the IASI observations, all the satellite pixels of the morning and evening orbits within a 200 km radius from the Brewer site have been averaged. The choice of radius was made since at an average wind speed of 6 m s^{-1} an air parcel will travel 250 km in 12 h, so with this spatial criteria we are including in the satellite averaging all pixels that might be overpassing the Brewer location within a temporal frame of 12 h (daytime). At the same time, the averaged IASI error and standard deviation have been computed. The results are presented in the scatter plot in Fig. 5. The linear fit is computed considering the IASI average error and a fixed error of 0.5 DU for the Brewer measurements. Note that the variability of the IASI SO_2 amount within 200 km is often much bigger then the IASI error bar. A correlation coefficient of 0.76 with root mean square differences of 1.16 DU has been found. This result is encouraging for the IASI retrieval, even if this initial comparison alone cannot be considered a comprehensive validation exercise because (1) it is difficult to assess the quality of Brewer SO_2 daily average values; (2) the comparison is restricted to the Eyjafjallajökull eruption, an eruption where the SO_2

ACPD
15, 24643–24693, 2015

plume covered a small range of altitudes (between 2 and 5 km) and a relative small loading amount.

From Fig. 5 it can be noted that for loadings up to and around 2 DU both types of observation appear to depict the same atmospheric SO_2 loading, which, depending on the location of the site, might be both of anthropogenic and volcanic provenance. For values between 2 and 3 DU there appears to be a slight underestimation by IASI instrument of around 0.5 DU, well within the statistical uncertainty. For higher loadings still, the Brewer instruments report higher SO_2 values than the satellite.

The overestimation of low amounts can be explained because the a priori SO_2 amount used by IASI retrieval is 0.5 DU. One factor that can explain the underestimation (by IASI of $SO_2 > 3$ DU) is that this IASI retrieval is sensitive to SO_2 values higher then the climatological SO_2 amount considered in the IASI data ensemble used to compute the error covariance matrix. In the case of the Eyjafallajökull eruption the north Atlantic and European region of April and May 2009 were used to compute the error covariance matrix, so the retrieval could be insensitive (biased) to the average values of SO_2 amount in that region, which includes the European background value of SO_2.

6 Total mass and vertical distribution

The SO_2 retrieval algorithm has been applied to several volcanic eruptions in the period 2008–2012. For each eruption the IASI orbits are grouped into twelve hour intervals in order to have, twice-daily maps, maps of IASI retrieved SO_2 amount and altitude.

These maps are regridded into a 0.125° lat/lon boxes. An example of maps for the Nabro eruption is shown in Fig. 6. Note that with only METOP-A the IASI data have a gap between the orbits at tropical latitudes, this gap is filled with the Metop-B launch in September 2012. It is also possible to have gaps in SO_2 coverage due to pixels that did not pass quality control. The regridding routine fills gaps by a triangular interpolation of neighbouring pixels.

ACPD
15, 24643–24693, 2015

Figure 6 shows an example of how the regridding routine fills in missing data. However, because of the possible creation of artefacts, the regridding should be used carefully. For example, in the case of a plume covering the edge of one orbit but with no plume present in the adjacent orbit, regridding can fill up the gaps between the orbits with a bigger plume than would be reasonable to expect. For the case studies presented here, all the regridded IASI maps have been inspected "by eye" to check that no particularly significant artefacts have been introduced.

The total SO_2 mass present in the atmosphere is obtained by summing all the values of the regularly gridded map of SO_2 amounts. In particular every grid-box column amount is multiplied by the grid-box area to obtain the SO_2 mass, and all the grid-box masses are summed together to obtain the total mass of SO_2 for each IASI image. The total mass errors are obtained in the same way from the grid box errors, i.e. all the box errors are summed to produce the total mass error. This is an overestimation of the error, but considering the mean squared error as total error will be an underestimation. This is due to the presence of systematic errors within the retrieval. The systematic errors are included within the error estimate but cannot be considered independent of each other, it is more likely that, if present, the systematic error will become a bias in the region and time considered. The time series of these total masses, together with the errors, are presented in Fig. 7 for the studied volcanic eruptions.

Using the IASI dataset it is possible to follow the plume evolution of several volcanic eruptions. Within the eruptions considered Nabro produced a maximum load of 1.6 Tg of SO_2, followed by Kasatochi (0.9 Tg), Grímsvötn (0.75 Tg), Copahue (0.72 Tg) and Sarychev (0.60 Tg).

From the eruptions presented in Fig. 7, there is a wide spread of error-bars, depending on the SO_2 amount, altitude and atmospheric conditions. In general, plumes tend to spread and dissipate with time, covering a larger area (i.e. more IASI pixels) with smaller quantities. This produces smaller SO_2 signals and consequently bigger retrieval errors. This is the main cause of the general tendency of increasing error bars with time.

ACPD
15, 24643–24693, 2015

It is also possible to estimate the SO_2 mass present between two altitude levels. Doing this every 0.5 km between 0 and 20 km gives a vertical distribution of SO_2 every ~ 12 h. These results are shown, in chronological order, in Figs. 8–11. Note that the colour-bars for different volcanic eruptions have different values, going from smaller values for Etna and Llaima eruptions to a maximum for Nabro. From these figures, it is possible to observe the temporal evolution of the SO_2 plume as a function of altitude. These plots have to be interpreted carefully and studied together with the maps of the amount and altitude (values and errors) because here the retrieved errors in altitude are not accounted for, and for low amounts of SO_2, error in altitude can be significant. Within the IASI spectra there is enough information to retrieve altitude from small/medium eruptions such as Etna and Nyamuragira/Nyiragongo.

The tropopause heights have been computed from ECMWF temperature and pressure profiles, using the lowest layer with a lapse rate below 2 K km^{-1} and lapse rate of 2 K km^{-1} in all layers within 2 km above this, for every pixel of the volcanic plume. The three tropopause lines, shown in Figs. 8–11, are the mean, and the mean plus or minus the standard deviations, within the IASI plume pixels in the 12 h maps. Within the plume, the tropopause heights can differ by many kilometres especially for plumes that cover a wide latitude range. As an example, the Kasatochi plume has been analysed between 30 and 90° N. Over this range of latitudes the tropopause height varies between 8 and 18 km. Given this caveat the lines of tropopause mean and standard deviation heights are indicative, e.g. a plume that is below the three lines is likely, but not necessary, confined to the troposphere, a plume that is above the three lines is likely confined in the stratosphere, and SO_2 that is between the lines could be in either the troposphere or stratosphere.

In the following Sects. 5.1–5.5 we describe the eruptions in Figs. 8–11 divided by geographic area. A summary of these comments together with other relevant literature and volcanic explosivity index (VEI) from Smithsonian is given in Table 1.

ACPD
15, 24643–24693, 2015

Three principal factors affect plume height: (i) the energetics of the eruption, (ii) the dynamic effect, (iii) retrieval artefacts in the case of a multilayer plumes. Here we attempt to discriminate between these factors as follows:

a. The energetics of the eruption. A crude parameter for eruption intensity and plume height is the "volcanic explosivity index" or VEI. We reported this, when availabe, in Table 1.

b. The dynamic effect. In the following sections we group the eruptions by geographic area in order to consider together eruptions that may have similar conditions of water vapour. Moreover we consider the tropopause altitude together with the plume altitude.

c. Retrieval artefact in the case of a multilayer plumes. We do not have a way to identify this in a fresh plume but we indicate (with a black triangle) when the old plume overpasses near the volcano again (with the possibility of presence of both the old overpassing plume and the new emitted plume, at two different altitudes). The vertical distribution plots in Figs. 8–11 present the studied eruptions in chronological order and indicate the presence of a new plume connected with the volcano with red triangular symbols at the bottom of the column.

6.1 Southern Chile: Llaima, Puyuhue-Cordon-Caulle and Copahue

In the Southern Hemisphere we analysed three eruptions that originated from volcanic activity in Chile. The wind direction was similar for each eruption so the SO_2 was transported to the east (towards South Africa).

Llaima (period analysed: 2–6 January 2008), is presented in Fig. 8. This is the smallest eruption in terms of SO_2 amount (with a maximum atmospheric load of 0.04 Tg) and after the first day, the plume was disconnected from the volcano.

Copahue (22–27 December 2012), in Fig. 11, release a higher amount of SO_2 (up to 0.72 Tg of atmospheric load) and there was a continuous plume from the volcano,

ACPD
15, 24643–24693, 2015

indicating that the volcano emitted SO_2 for at least seven days. Both of these eruptions remained confined to the troposphere.

The Puyehue-Cordon-Caulle eruption of 5–30 June 2011 was the most significant eruption in southern Chile since 1991. The eruption commenced with the formation of a very significant eruption plume, that was tracked around the globe, and sustained, lower-level activity that continued intermittently during the observation period. This eruption was between Llaima and Copahue in terms of SO_2 amount (maximum load of 0.13 Tg), but higher than both in terms of VEI (with a value of 5), and with a much higher altitude (Fig. 11). The first part of the eruption produced a higher plume in terms of amount and altitude, and a lower plume connected with the volcano was present intermittently for all of the period observed. The maximum amount of SO_2 loading found was 0.13 ± 0.06 Tg on 8 and 9 June. Theys et al. (2013) present the SO_2 amount from the Clarisse et al. (2012) IASI scheme, assuming an altitude of 13 km, and reported values around 0.14 Tg (and higher) for the periods 6–9 June, with a maximum on 7 June. The fresh part of the plume (over south America and the western Atlantic ocean) is found to be significantly lower using C12 (between 2 and 5 km of altitude) than the altitude of 13 km assumed by Theys et al. (2013), and the SO_2 amount for a plume at 5 km will be underestimated using the assumption of higher altitude. Due to the opposite effect, the presence of SO_2 higher then 13 km in the first two days may explain the discrepancy in the SO_2 load (Fig. 2 from Theys et al., 2013 reports higher SO_2 than C12 but assumes lower altitude than C12).

6.2 Northern Pacific Ocean: Okmok, Kasatochi and Sarychev

Okmok, Kasatochi and Sarychev eruptions (Figs. 8 and 9) all affected the boreal atmosphere and injected SO_2 to altitudes around the tropopause (and higher).

Okmok (12–20 July 2008) injected SO_2 around 12 km and the plume spread south and east from the volcano, over the Pacific Ocean. The main plume reached the US and Canada, and there was an intermittent presence of a small and low plume connected with the volcano.

ACPD
15, 24643–24693, 2015

Kasatochi (7–22 August 2008) injected the majority amount of SO_2 within the first three days and the plume spread around the Northern Hemisphere, going east, north and west from the volcano. The SO_2 amount reached a maximum seven days after the start of eruption, indicating continuous injection from the volcano. Within the first ten days of the eruption it affected the latitude bands 30 to 90° N. The SO_2 amounts for the first days of the eruption are in the ranges reported from Corradini et al. (2010) for AIRS and MODIS estimate. (Corradini et al., 2010 report AIRS and MODIS 7.3 µm SO_2 mass loadings between 0.3 and 1.2 Tg, while the MODIS ash corrected 8.7 µm SO_2 masses vary between 0.4 and 2.7 Tg). The altitude retrieved using C12 for Kasatochi is consistent with 12.5 ± 4 km reported by Karagulian et al. (2010), but the total SO_2 load is around 30 % lower. Karagulian et al. (2010) use an IASI retrieval from ν_3 band (1362 cm^{-1}) and $\nu_1 + \nu_3$ band (2500 cm^{-1}). The altitudes from C12 are also comparable with the range reported in CALIPSO and OMI data from Wang et al. (2013) (Wang et al., 2013 used the OMI retrieval of altitude and amount and GEOS-Chem models to estimate that the forcing by Kasatochi volcanic sulphate aerosol became negligible six months after the eruption).

Sarychev is located at a similar latitude to Kasatochi, but in the Kurile islands south of Kamchatka. The IASI SO_2 scheme, C12, (similar to that previously reported by the Université Libre de Bruxelles, IASI-ULB, near real-time SO_2 alert system, http://cpm-ws4.ulb.ac.be/Alerts/index.php, Rix et al., 2009; Haywood et al., 2010), retrieves a small tropospheric plume in the two images from 11 June 2009, followed by a higher plume on 12 June. The SO_2 loading increased in the following days (with a big injection the 15 June 2009) reaching a maximum on 16 June (0.6 Tg). Then the SO_2 load remained approximately constant for 16–18 June, before decrasig after that. The plume went in two directions, one branch spreading across the Pacific Ocean to North America and crossing Canada, reaching the Atlantic Ocean on 22 June and the Spanish coast of Europe on 24 June; the second branch went north, crossing Siberia up to the Siberian Sea and turning east to Greenland.

ACPD
15, 24643–24693, 2015

6.3 Africa: Dalafilla, Nabro

Two volcanic eruptions from the the Ethiopian Rift, Dalafilla in November 2008 and Nabro in June 2011, had a lower plume around 4–6 km and a higher part of the plume around the tropopause, but they were nearly one order of magnitude different in terms of SO_2 amount. Dalafilla produced a maximum SO_2 atmospheric loading of 0.2 Tg while Nabro produced 1.6 Tg. This could be the result of volcanic effects (for example Dalafilla was a very short-lived and vigorous fire-fountaining eruption from an extended fissure that produced, in some parts low mass eruption rates and in other parts much higher eruption rates. Another possible explanation of how a medium/small eruption such as Dalafilla (VEI 3) reached the tropopause altitude is illustrated in Tupper et al. (2009) and implicate the effect of a moist atmosphere. Tupper et al. (2009) showed that volcanic emissions with different eruption rates in moist atmosphere both reached the tropopause; in dry atmosphere they reach different altitudes.

The first IASI observation showing the Dalafilla eruption was at 05:00 UTC on 4 November 2008. The plume is divided into a lower and a higher part. These spread north and east from Ethiopia, covering the Arabic peninsula, and arrived over north India and the Himalayas on the 5 November. They spread then over China and a diluted plume arrived over south Japan on 6 November. IASI detected SO_2 near the volcano in every image in this period. According to Meteosat-9 false color RGB images, the eruption started between 12:45 UTC and 13:00 UTC on 3 November 2008, with high-level SO_2 plumes and an ash plume (mixed with ice). The low-level SO_2 plume, started three hours later[2].

The IASI images of SO_2 amount and altitude are consistent with the measurements over northern India reported by Mallik et al. (2013). In particular Mallik et al. (2013) report: (i) high concentration of column SO_2 from ground measurements where the time of exceptionally high SO_2 amount is consistent with the IASI plume arriving over the Indian location; (ii) CALIPSO observations of a scattering feature around 4–5 km

[2] http://www.eumetsat.int/website/home/Images/ImageLibrary/DAT_IL_08_11_03_A.html

ACPD
15, 24643–24693, 2015

altitude on 6 November that is consistent with the lower part of the plume reported here by IASI; (iii) OMI maps, obtained assuming a fixed altitude, with a position of the SO_2 plume similar to IASI. With the use of C12 IASI scheme it is possible to discern that there is both a lower plume in the troposphere (as reported by Mallik et al., 2013) and a significant part of the plume at altitudes around the tropopause.

Nabro produced the largest amount of SO_2 in any volcanic plume observed by IASI with a maximum of up to 1.6 ± 0.3 Tg of SO_2.

Numerous previouse studies have documented this eruption, with many of these focusing on whether Nabro inject SO_2 directly into the stratosphere or whether the injection was associated with monsoon circulation (Bourassa et al., 2012, 2013; Sawamura et al., 2012; Vernier et al., 2013; Fromm et al., 2013, 2014; Clarisse et al., 2014; Biondi et al., 2015). A more detailed study of the Nabro Eruption, also using the C12 IASI retrieval scheme, is reported in Fromm et al. (2014), and concluded that "Nabro injected sulphur directly to or above the tropopause upon the initial eruption on 12/13 June, and again on 16 June 2011". Here we include the Nabro summary of the C12 IASI dataset. The Nabro plume is retrieved on 13 June, with a plume over north-east Africa between 14 and 18 km height. On the 14 the plume arrived over the Middle East and over central Asia on 15 June. The eruption formed two plumes at different altitudes, the higher one that reached the stratosphere and a lower one that remained confined to the troposphere with less then 10 km altitude. The higher plume is further separated into two segments, a "north" one (15 km and above) and a "south" one, a bit lower. Over all these days the plume was still attached to the volcano, indicating continuous injection. On 17 June there is a lower altitude plume and a new high altitude part going over north-east Africa.

In Fromm et al. (2014) two comparisons have demonstrated the consistency of IASI altitude with other measurements: (1) morning and afternoon IASI data of the 14 June are compared with the lidar ground data at Sede Boker (Israel) and an SO_2 profile from MLS (Fromm et al., 2014; Fig. 8); (2) the night time IASI measurements of 17 June are compared with the Caliop and MLS measurements (Fromm et al., 2014; Fig. 9).

ACPD
15, 24643–24693, 2015

6.4 Iceland: Eyjafjallajökull and Grímsvötn

Eruptions of Eyjafjallajökull in April and May 2010 and Grímsvötn in May 2011 have been examined. A deeper analysis of the IASI SO_2 plume from the Eyjafjallajökull eruption is presented in Carboni et al. (2012) and here we only report the time series of vertical distribution.

The first IASI observation of the Eyjafjallajökull plume is in the evening of 14 April 2010. The SO_2 plume altitudes retrieved in successive observations up to 20 April are below 10 km, mainly confined below 5 km. Small amounts of SO_2 between 16 and 20 April are between 5 and 10 km in altitude. From 20 to 30 April SO_2 is always below 5 km. There is a little increase of SO_2 amount and altitude on the 1 and 2 May, and a more pronounced increase of both SO_2 amount and altitude from the 5 May. The retrieved altitude has a maximum during the 14–17 May period, where values reach around 10 km.

Grímsvötn's plume was first observed by IASI on the morning of 22 May 2011. From the afternoon of the 22 it is possible to see an SO_2 rich plume going north, with a segment going north-east, and a lower plume going south/south-east. The denser part of the higher SO_2 plume moved west and arrived over Greenland, and out of the analysed area on 24 May. This segment re-entered the analysed area on 26 May in the afternoon (this is why the last column of the plot has an apparent increase in SO_2). The lower altitude plume, moving in south/south-east direction, is reported to be more ash rich (Moxnes et al., 2014) and travelled toward Europe, arriving over the northern UK on the 24 in the morning, and over Scandinavia in the afternoon. These observations of the Grímsvötn eruption do not completely represent the total atmospheric SO_2 due to the fact that a part of the plume is missing.

6.4.1 Minor frequent events: Etna and Congo

The activity of Etna and Nyamuragira/Nyiragongo during the period was limited to smaller eruptions and lava-fountains. Here we do not report an exhaustive list of these

ACPD
15, 24643–24693, 2015

episodes, but a few examples to show how these emissions can be observed by IASI. The Smithsonian Institution reported that Nyamuragira erupted on 2 January 2010 and 6 November 2011. From IASI data it is not possible to distinguish between Nyamuragira and Nyriagongo emissions, but SO_2 plumes are observed from 3 to 12 January 2010 and from 7 to 15 November 2011. The SO_2 plumes spread over the equatorial area of Africa from Congo up to Sudan and Chad, with decreasing SO_2 loading away from the volcano. The main plumes were confined to the troposphere and disappeared after a few days.

The Etna events considered are the 23–25 November 2007 eruption and the 2011 lava-fountains: 11–13 January, 17–19 February, 9–12 April, 11–13 May, 8–10 July, 18–20 July, 24–26 July, 29 July, 1 August, 4–7 August, 11–13 August, 19–21 August, 28–30 August, 7–10 September, 18–20 September, 27–30 September, 12–17 November. Analysis was performed for the lava fountain period plus one day either side. The Etna eruption in 2007 produced the highest SO_2 atmospheric loading for the period analysed (more then 0.1 Tg). The lava-fountains are associated with smaller amounts of SO_2 and with large error. Etna emissions are approximately ten times smaller then those from the Congo. In particular, the SO_2 for 2011 Etna fountains have been validated within the SAMSH-SACS2 project and the SO_2 amount measured by IASI are consistent with ground observation (Spinetti et al., 2014).

7 Conclusions

In this paper, the IASI SO_2 volcanic plume altitudes and amount from a recently developed SO_2 retrieval algorithm (Carboni et al., 2012) are presented. IASI has significant advantages for the monitoring of extended volcanic eruptions, because it can be used to track the intensity of the eruption, both in terms of gas amount and gas plume height.

Comparisons of IASI altitudes against CALIPSO profiles and IASI SO_2 column amounts against Brewer ground measurements have been performed. These show that IASI retrieved values are consistent with the satellite and ground measurements.

ACPD
15, 24643–24693, 2015

Despite the ability of IASI to retrieve the plume altitude, it could be difficult to distinguish, with only IASI data, if the eruption injects into the stratosphere or into the high troposphere. Further work integrating and comparing IASI with other measurements, such as lidar or limb Michelson Interferometer for Passive Atmospheric Sounding (MIPAS) measurements, are needed to better assess the ability of IASI to determine injection into the stratosphere.

The IASI scheme has been used to follow the vertical distribution of SO_2 as a function of time (twice daily), for different eruption types (e.g. VEI ranging between 1 and 5) and different latitudes. This work demonstrates that while VEI is a convenient and rapidly estimated proxy for eruption "scale", it is a poor index of the potential height to which volcanic SO_2 is injected.

There is a tendency for volcanic SO_2 plumes to reach a point of buoyancy near the tropopause. All of the eruptions in the tropics (except Nyamuragira), reached the tropopause. In the mid latitudes, the eruptions of Eyjafjallajökull, Llaima, Copahue and Etna remained confined in the troposphere.

Acknowledgements. E. Carboni, R. Grainger, T. A. Mather and D.M. Pyle were supported by the NERC Centre for Observation and Modelling of Earthquakes, Volcanoes, and Tectonics (COMET).

References

Aiuppa, A., Cannata, A., Cannavo, F., Di Grazia, G., Ferrari, F., Giudice, G., Gurrieri, S., Liuzzo, M., Mattia, M., Montalto, P., Patan, D., and Puglisi, G.: Patterns in the recent 2007–2008 activity of Mount Etna volcano investigated by integrated geophysical and geochemical observations, Geochem. Geophy. Geosy., 11, Q09008, doi:10.1029/2010GC003168, 2010. 24681

Behncke, B., Branca, S., Corsaro, R., De Beni, E., Miraglia, L., and Proietti, C.: The 2011–2012 summit activity of Mount Etna: birth, growth and products of the new SE crater, J. Volcanol. Geoth. Res., 270, 10–21, doi:10.1016/j.jvolgeores.2013.11.012, 2014. 24681

ACPD
15, 24643–24693, 2015

Bignami, C., Corradini, S., Merucci, L., De Michele, M., Raucoules, D., De Astis, G., Stramondo, S., and Piedra, J.: Multisensor satellite monitoring of the 2011 Puyehue-Cordon Caulle Eruption, IEEE J. Sel. Top. Appl., 7, 2786, doi:10.1109/JSTARS.2014.2320638, 2014. 24682

Biondi, R., Steiner, A., Kirchengast, G., Brenot, H., and Rieckh, T.: A novel technique including GPS radio occultation for detecting and monitoring volcanic clouds, Geophys. Res. Lett., in revision, 2015. 24662, 24682

Bitar, L., Duck, T., Kristiansen, N., Stohl, A., and Beauchamp, S.: Lidar observations of Kasatochi volcano aerosols in the troposphere and stratosphere, J. Geophys. Res.-Atmos., 115, D00L13, doi:10.1029/2009JD013650, 2010. 24679

Blumstein, D., Chalon, G., Carlier, T., Buil, C., Hebert, P., Maciaszek, T., Ponce, G., Phulpin, T., Tournier, B., Simeoni, D., Astruc, P., Clauss, A., Kayal, G., and Jegou, R.: IASI instrument: technical overview and measured performances, Proceedings of SPIE – The International Society for Optical Engineering, 5543, 196–207, doi:10.1117/12.560907, 2004. 24648

Bluth, G. and Carn, S.: Exceptional sulfur degassing from Nyamuragira volcano, 1979–2005, Int. J. Remote Sens., 29, 6667–6685, doi:10.1080/01431160802168434, 2008. 24681

Boichu, M., Menut, L., Khvorostyanov, D., Clarisse, L., Clerbaux, C., Turquety, S., and Coheur, P.-F.: Inverting for volcanic SO_2 flux at high temporal resolution using spaceborne plume imagery and chemistry-transport modelling: the 2010 Eyjafjallajökull eruption case study, Atmos. Chem. Phys., 13, 8569–8584, doi:10.5194/acp-13-8569-2013, 2013. 24680

Bonadonna, C., Folch, A., Loughlin, S., and Puempel, H.: Future developments in modelling and monitoring of volcanic ash clouds: outcomes from the first IAVCEI-WMO workshop on ash dispersal forecast and civil aviation, B. Volcanol., 74, 1–10, doi:10.1007/s00445-011-0508-6, 2012. 24645

Bonali, F.: Earthquake-induced static stress change on magma pathway in promoting the 2012 Copahue eruption, Tectonophysics, 608, 127–137, doi:10.1016/j.tecto.2013.10.006, 2013. 24682

Bourassa, A., Robock, A., Randel, W., Deshler, T., Rieger, L. A., Lloyd, N., Llewellyn, E., and Degenstein, D.: Large volcanic aerosol load in the stratosphere linked to asian monsoon transport, Science, 337, 78–81, doi:10.1126/science.1219371, 2012. 24662, 24682

Bourassa, A., Robock, A., Randel, W., Deshler, T., Rieger, L., Lloyd, N., Llewellyn, E., and Degenstein, D.: Response to comments on “large volcanic aerosol load in the stratosphere

ACPD
15, 24643–24693, 2015

linked to Asian monsoon transport", Science, 339, 647, doi:10.1126/science.1227961, 2013. 24662, 24682

Brenot, H., Theys, N., Clarisse, L., van Geffen, J., van Gent, J., Van Roozendael, M., van der A, R., Hurtmans, D., Coheur, P.-F., Clerbaux, C., Valks, P., Hedelt, P., Prata, F., Rasson, O., Sievers, K., and Zehner, C.: Support to Aviation Control Service (SACS): an online service for near-real-time satellite monitoring of volcanic plumes, Nat. Hazards Earth Syst. Sci., 14, 1099–1123, doi:10.5194/nhess-14-1099-2014, 2014. 24645

Budi-Santoso, A., Lesage, P., Dwiyono, S., Sumarti, S., Subandriyo, Surono, Jousset, P., and Metaxian, J.-P.: Analysis of the seismic activity associated with the 2010 eruption of Merapi Volcano, Java, J. Volcanol. Geoth. Res., 261, 153–170, doi:10.1016/j.jvolgeores.2013.03.024, 2013. 24680

Calabrese, S., Aiuppa, A., Allard, P., Bagnato, E., Bellomo, S., Brusca, L., D'Alessandro, W., and Parello, F.: Atmospheric sources and sinks of volcanogenic elements in a basaltic volcano (Etna, Italy), Geochim. Cosmochim. Ac., 75, 7401–7425, doi:10.1016/j.gca.2011.09.040, 2011. 24645

Campion, R.: New lava lake at Nyamuragira volcano revealed by combined ASTER and OMI SO_2 measurements, Geophys. Res. Lett., 41, 7485–7492, doi:10.1002/2014GL061808, 2014. 24681

Campion, R., Salerno, G., Coheur, P.-F., Hurtmans, D., Clarisse, L., Kazahaya, K., Burton, M., Caltabiano, T., Clerbaux, C., and Bernard, A.: Measuring volcanic degassing of SO_2 in the lower troposphere with ASTER band ratios, J. Volcanol. Geoth. Res., 194, 42–54, doi:10.1016/j.jvolgeores.2010.04.010, 2010. 24646

Carboni, E., Grainger, R., Walker, J., Dudhia, A., and Siddans, R.: A new scheme for sulphur dioxide retrieval from IASI measurements: application to the Eyjafjallajökull eruption of April and May 2010, Atmos. Chem. Phys., 12, 11417–11434, doi:10.5194/acp-12-11417-2012, 2012. 24647, 24648, 24663, 24664, 24680

Carn, S. A. and Bluth, G. J. S.: Prodigious sulfur dioxide emissions from Nyamuragira volcano, D. R. Congo, Geophys. Res. Lett., 30, 2211, doi:10.1029/2003GL018465, 2003. 24681

Carn, S. A., and Prata, F. J.: Satellite-based constraints on explosive SO_2 release from Soufriere Hills Volcano, Montserrat, Geophys. Res. Lett., 37, L00E22, doi:10.1029/2010GL044971, 2010. 24680

ACPD
15, 24643–24693, 2015

Carn, S., Krueger, A., Krotkov, N., Yang, K., and Evans, K.: Tracking volcanic sulfur dioxide clouds for aviation hazard mitigation, Nat. Hazards, 51, 325–343, doi:10.1007/s11069-008-9228-4, 2009. 24646

Carn, S., Krotkov, N., Yang, K., and Krueger, A.: Measuring global volcanic degassing with the ozone monitoring instrument (OMI), Geol. Soc. Sp., 380, 229–257, doi:10.1144/SP380.12, 2013. 24681

Carn, S. A. and Lopez, T. M.: Opportunistic validation of sulfur dioxide in the Sarychev Peak volcanic eruption cloud, Atmos. Meas. Tech., 4, 1705–1712, doi:10.5194/amt-4-1705-2011, 2011. 24680

Carn, S. A., Krueger, A. J., Bluth, G. J. S., Schaefer, S. J., Krotkov, N. A., Watson, I. M., and Datta, S.: Volcanic eruption detection by the Total Ozone Mapping Spectrometer (TOMS) instrument: a 22-year record of sulfur dioxide and ash emissions, in: Volcanic Degassing, edited by: Oppenheimer, C., Pyle, D. M., and Barclay, J., vol. 213, Geological Society, London, 177–203, 2003. 24646

Christopher, T., Edmonds, M., Humphreys, M., and Herd, R.: Volcanic gas emissions from Soufriere Hills Volcano, Montserrat 1995–2009, with implications for mafic magma supply and degassing, Geophys. Res. Lett., 37, L00E04, doi:10.1029/2009GL041325, 2010. 24680

Christopher, T., Edmonds, M., Taisne, B., Odbert, H., Costa, A., Hards, V., and Wadge, G.: Periodic sulphur dioxide degassing from the Soufriere Hills Volcano related to deep magma supply, Geological Society, London, Special Publications, 410, doi:10.1144/SP410.11, 2014. 24680

Clarisse, L., Hurtmans, D., Clerbaux, C., Hadji-Lazaro, J., Ngadi, Y., and Coheur, P.-F.: Retrieval of sulphur dioxide from the infrared atmospheric sounding interferometer (IASI), Atmos. Meas. Tech., 5, 581–594, doi:10.5194/amt-5-581-2012, 2012. 24659

Clarisse, L., Coheur, P.-F., Theys, N., Hurtmans, D., and Clerbaux, C.: The 2011 Nabro eruption, a SO_2 plume height analysis using IASI measurements, Atmos. Chem. Phys., 14, 3095–3111, doi:10.5194/acp-14-3095-2014, 2014. 24647, 24662, 24682

Clerbaux, C., Coheur, P.-F., Clarisse, L., Hadji-Lazaro, J., Hurtmans, D., Turquety, S., Bowman, K., Worden, H., and Carn, S.: Measurements of SO_2 profiles in volcanic plumes from the NASA Tropospheric Emission Spectrometer (TES), Geophys. Res. Lett., 35, L22807, doi:10.1029/2008GL035566, 2008. 24647

Clerbaux, C., Boynard, A., Clarisse, L., George, M., Hadji-Lazaro, J., Herbin, H., Hurtmans, D., Pommier, M., Razavi, A., Turquety, S., Wespes, C., and Coheur, P.-F.: Monitoring of atmo-

ACPD
15, 24643–24693, 2015

spheric composition using the thermal infrared IASI/MetOp sounder, Atmos. Chem. Phys., 9, 6041–6054, doi:10.5194/acp-9-6041-2009, 2009. 24648

Corradini, S., Merucci, L., and Prata, A. J.: Retrieval of SO_2 from thermal infrared satellite measurements: correction procedures for the effects of volcanic ash, Atmos. Meas. Tech., 2, 177–191, doi:10.5194/amt-2-177-2009, 2009. 24646

Corradini, S., Merucci, L., Prata, A. J., and Piscini, A.: Volcanic ash and SO_2 in the 2008 Kasatochi eruption: retrievals comparison from different IR satellite sensors, J. Geophys. Res., 115, D00L21, doi:10.1029/2009JD013634, 2010. 24660, 24679

Costa, F., Andreastuti, S., Bouvet de Maisonneuve, C., and Pallister, J.: Petrological insights into the storage conditions, and magmatic processes that yielded the centennial 2010 Merapi explosive eruption, J. Volcanol. Geoth. Res., 261, 209–235, doi:10.1016/j.jvolgeores.2012.12.025, 2013. 24680

Cronin, S., Lube, G., Dayudi, D., Sumarti, S., Subrandiyo, S., and Surono: Insights into the October–November 2010 Gunung Merapi eruption (Central Java, Indonesia) from the stratigraphy, volume and characteristics of its pyroclastic deposits, J. Volcanol. Geoth. Res., 261, 244–259, doi:10.1016/j.jvolgeores.2013.01.005, 2013. 24680

Cuoco, E., Tedesco, D., Poreda, R., Williams, J., De Francesco, S., Balagizi, C., and Darrah, T.: Impact of volcanic plume emissions on rain water chemistry during the January 2010 Nyamuragira eruptive event: implications for essential potable water resources, J. Hazard. Mater., 244–245, 570–581, doi:10.1016/j.jhazmat.2012.10.055, 2013. 24681

De Muer, D. and De Backer, H.: Revision of 20 years of Dobson total ozone data at Uccle (Belgium): fictitious Dobson total ozone trends induced by sulfur dioxide trends, J. Geophys. Res.-Atmos., 97, 5921–5937, doi:10.1029/91JD03164, 1992. 24653

Delmelle, P.: Environmental impacts of tropospheric volcanic gas plumes, Geol. Soc. Sp., 213, 381–399, doi:10.1144/GSL.SP.2003.213.01.23, 2003. 24645

Delmelle, P., Stix, J., Baxter, P. J., Garcia-Alvarez, J., and Barquero, J.: Atmospheric dispersion, environmental effects and potential health hazard associated with the low-altitude gas plume of Masaya volcano, Nicaragua, B. Volcanol., 64, 423–434, doi:10.1007/s00445-002-0221-6, 2002. 24645

Doeringer, D., Eldering, A., Boone, D., Gonzalez Abad, G., and Bernath, P.: Observation of sulfate aerosols and SO_2 from the Sarychev volcanic eruption using data from the Atmospheric Chemistry Experiment (ACE), J. Geophys. Res., 117, D03203, doi:10.1029/2011JD016556, 2012. 24680

ACPD
15, 24643–24693, 2015

Ebmeier, S. K., Sayer, A. M., Grainger, R. G., Mather, T. A., and Carboni, E.: Systematic satellite observations of the impact of aerosols from passive volcanic degassing on local cloud properties, Atmos. Chem. Phys., 14, 10601–10618, doi:10.5194/acp-14-10601-2014, 2014. 24645

Encinas-Oropesa, A., Drew, G., Hardy, M., Leggett, A., Nicholls, J., and Simms, N.: Effects of oxidation and hot corrosion in a nickel disc alloy, in: Superalloys Conference Proceedings, 609–618, 2008. 24645

Flemming, J. and Inness, A.: Volcanic sulfur dioxide plume forecasts based on UV satellite retrievals for the 2011 Grimsvotn and the 2010 Eyjafjallajökull eruption, J. Geophys. Res.-Atmos., 118, 10172–10189, doi:10.1002/jgrd.50753,2, 2013. 24645, 24682

Fromm, M., Nedoluha, G., and Charvát, Z.: Comment on 'Large volcanic aerosol load in the stratosphere linked to Asian monsoon transport", Science, 339, 647, doi:10.1126/science.1228605, 2013. 24662, 24682

Fromm, M., Kablick, G., Nedoluha, G., Carboni, E., Grainger, R., Campbell, J., and Lewis, J.: Correcting the record of volcanic stratospheric aerosol impact: Nabro and Sarychev Peak, J. Geophys. Res., 119, 10343–10364, doi:10.1002/2014JD021507, 2014. 24662, 24680, 24682

Glasow, R. V.: Atmospheric chemistry in volcanic plumes, P. Natl. Acad. Sci. USA, 107, 6594–6599, doi:10.1073/pnas.0913164107, 2010. 24645

Graf, H.-F., Feichter, J., and Langmann, B.: Volcanic sulfur emissions: estimates of source strength and its contribution to the global sulfate distribution, J. Geophys. Res.-Atmos., 102, 10727–10738, doi:10.1029/96JD03265, 1997. 24645

Guerrieri, L., Merucci, L., Corradini, S., and Pugnaghi, S.: Evolution of the 2011 Mt. Etna ash and SO_2 lava fountain episodes using SEVIRI data and VPR retrieval approach, J. Volcanol. Geoth. Res., 291, 63–71, doi:10.1016/j.jvolgeores.2014.12.016, 2015. 24681

Haywood, J., Jones, A., Clarisse, L., Bourassa, A., Barnes, J., Telford, P., Bellouin, N., Boucher, O., Agnew, P., Clerbaux, C., Coheur, P., Degenstein, D., and Braesicke, P.: Observations of the eruption of the Sarychev volcano and simulations using the HadGEM2 climate model, J. Geophys. Res.-Atmos., 115, D21212, doi:10.1029/2010JD014447, 2010. 24680

Höpfner, M., Glatthor, N., Grabowski, U., Kellmann, S., Kiefer, M., Linden, A., Orphal, J., Stiller, G., von Clarmann, T., Funke, B., and Boone, C. D.: Sulfur dioxide (SO_2) as observed

ACPD
15, 24643–24693, 2015

by MIPAS/Envisat: temporal development and spatial distribution at 15–45 km altitude, Atmos. Chem. Phys., 13, 10405–10423, doi:10.5194/acp-13-10405-2013, 2013. 24646

Innocenti, S., Andreastuti, S., Furman, T., del Marmol, M.-A., and Voight, B.: The pre-eruption conditions for explosive eruptions at Merapi volcano as revealed by crystal texture and mineralogy, J. Volcanol. Geoth. Res., 261, 69–86, doi:10.1016/j.jvolgeores.2012.12.028, 2013a. 24680

Innocenti, S., del Marmol, M.-A., Voight, B., Andreastuti, S., and Furman, T.: Textural and mineral chemistry constraints on evolution of Merapi Volcano, Indonesia, J. Volcanol. Geoth. Res., 261, 20–37, 2013b. 24680

Jenkins, S., Komorowski, J.-C., Baxter, P., Spence, R., Picquout, A., Lavigne, F., and Surono: The Merapi 2010 eruption: an interdisciplinary impact assessment methodology for studying pyroclastic density current dynamics, J. Volcanol. Geoth. Res., 261, 316–329, doi:10.1016/j.jvolgeores.2013.02.012, 2013. 24680

Karagulian, F., Clarisse, L., Clerbaux, C., Prata, A. J., Hurtmans, D., and Coheur, P. F.: Detection of volcanic SO_2, ash, and H_2SO_4 using the Infrared Atmospheric Sounding Interferometer (IASI), J. Geophys. Res., 115, D00L02, doi:10.1029/2009JD012786, 2010. 24660, 24679

Kerr, J., McElroy, C., and Olafson, R.: Measurements of ozone with the Brewer spectrophotometer, in: Proceedings of the Quadrennial International Ozone Symposium, edited by: London, J., Natl. Cent. for Atmos. Res., Boulder, Colo., vol. 1, 74–79, 1981. 24653

Koukouli, M. E., Clarisse, L., E., C., van Gent, J., C., S., Balis, D., Dimopoulos, S., R. G.3, G., Theys, N., Tampellini, L., and Zehner, C.: Intercomparison of Metop-A SO_2 measurements during the 2010–2011 Icelandic eruptions, Ann. Geophys.-Italy, 57, doi:10.4401/ag-6613, 2014. 24647, 24653, 24682

Kristiansen, N., Stohl, A., Prata, A., Richter, A., Eckhardt, S., Seibert, P., Hoffmann, A., Ritter, C., Bitar, L., Duck, T., and Stebel, K.: Remote sensing and inverse transport modeling of the Kasatochi eruption sulfur dioxide cloud, J. Geophys. Res.-Atmos., 115, D00L16, doi:10.1029/2009JD013286, 2010. 24679

Kroll, J., Cross, E., Hunter, J., Pai, S., TREX XII, TREX XI, Wallace, L., Croteau, P., Jayne, J., Worsnop, D., Heald, C., Murphy, J., and Frankel, S.: Atmospheric evolution of sulfur emissions from Kilauea: real-time measurements of oxidation, dilution, and neutralization within a volcanic plume, Environ. Sci. Technol., 49, 4129–4137, doi:10.1021/es506119x, 2015. 24645

ACPD
15, 24643–24693, 2015

Krotkov, N., Cam, S., Krueger, A., Bhartia, P., and Yang, K.: Band residual difference algorithm for retrieval of SO_2 from the aura Ozone Monitoring Instrument (OMI), IEEE T. Geosci. Remote, 44, 1259–1266, doi:10.1109/TGRS.2005.861932, 2006. 24646

Krotkov, N., Schoeberl, M., Morris, G., Carn, S., and Yang, K.: Dispersion and lifetime of the SO_2 cloud from the August 2008 Kasatochi eruption, J. Geophys. Res.-Atmos., 115, D00L20, doi:10.1029/2010JD013984, 2010. 24679

Luehr, B.-G., Koulakov, I., Rabbel, W., Zschau, J., Ratdomopurbo, A., Brotopuspito, K., Fauzi, P., and Sahara, D.: Fluid ascent and magma storage beneath Gunung Merapi revealed by multi-scale seismic imaging, J. Volcanol. Geoth. Res., 261, 7–19, doi:10.1016/j.jvolgeores.2013.03.015, 2013. 24680

Mallik, C., Lal, S., Naja, M., Chand, D., Venkataramani, S., Joshi, H., and Pant, P.: Enhanced SO_2 concentrations observed over northern India: Role of long-range transport, Int. J. Remote Sens., 34, 2749–2762, doi:10.1080/01431161.2012.750773, 2013. 24661, 24679

Marzano, F. S., Lamantea, M., Montopoli, M., Di Fabio, S., and Picciotti, E.: The Eyjafjöll explosive volcanic eruption from a microwave weather radar perspective, Atmos. Chem. Phys., 11, 9503–9518, doi:10.5194/acp-11-9503-2011, 2011. 24680

Mather, T., Pyle, D., and Oppenheimer, C.: Tropospheric volcanic aerosol, in: Volcanism and the Earth's Atmosphere, Geophysical Monograph 139, edited by: Robock, A. and Oppenheimer, C., Am. Geophys. Union, Washington, DC, 189–212, doi:10.1029/139GM12, 2003. 24645

McCormick, B., Edmonds, M., Mather, T., Campion, R., Hayer, C., Thomas, H., and Carn, S.: Volcano monitoring applications of the ozone monitoring instrument, Geol. Soc. Sp., 380, 259–291, doi:10.1144/SP380.11, 2013. 24679

McGonigle, A. J. S., Delmelle, P., Oppenheimer, C., Tsanev, V. I., Delfosse, T., Williams-Jones, G., Horton, K., and Mather, T. A.: SO_2 depletion in tropospheric volcanic plumes, Geophys. Res. Lett., 31, L13201, doi:10.1029/2004GL019990, 2004. 24645

Moxnes, E., Kristiansen, N., Stohl, A., Clarisse, L., Durant, A., Weber, K., and Vogel, A.: Separation of ash and sulfur dioxide during the 2011 Grímsvötn eruption, J. Geophys. Res.-Atmos-, 119, 7477–7501, doi:10.1002/2013JD021129, 2014. 24663, 24682

Nicholson, E., Mather, T., Pyle, D., Odbert, H., and Christopher, T.: Cyclical patterns in volcanic degassing revealed by SO_2 flux timeseries analysis: an application to Soufriére Hills Volcano, Montserrat, Earth Planet. Sc. Lett., 375, 209–221, doi:10.1016/j.epsl.2013.05.032, 2013. 24680

ACPD
15, 24643–24693, 2015

Nowlan, C. R., Liu, X., Chance, K., Cai, Z., Kurosu, T. P., Lee, C., and Martin, R. V.: Retrievals of sulfur dioxide from the Global Ozone Monitoring Experiment 2 (GOME-2) using an optimal estimation approach: algorithm and initial validation, J. Geophys. Res., 116, D18301, doi:10.1029/2011JD015808, 2011. 24646, 24648, 24679

Pagli, C., Wright, T., Ebinger, C., Yun, S.-H., Cann, J., Barnie, T., and Ayele, A.: Shallow axial magma chamber at the slow-spreading Erta Ale Ridge, Nat. Geosci., 5, 284–288, doi:10.1038/ngeo1414, 2012. 24679

Pallister, J., Schneider, D., Griswold, J., Keeler, R., Burton, W., Noyles, C., Newhall, C., and Ratdomopurbo, A.: Merapi 2010 eruption-Chronology and extrusion rates monitored with satellite radar and used in eruption forecasting, J. Volcanol. Geoth. Res., 261, 144–152, doi:10.1016/j.jvolgeores.2012.07.012, 2013. 24680

Patane, D., Aiuppa, A., Aloisi, M., Behncke, B., Cannata, A., Coltelli, M., Di Grazia, G., Gambino, S., Gurrieri, S., Mattia, M., and Salerno, G.: Insights into magma and fluid transfer at Mount Etna by a multiparametric approach: A model of the events leading to the 2011 eruptive cycle, J. Geophys. Res.-Solid, 118, 3519–3539, doi:10.1002/jgrb.50248, 2013. 24681

Petersen, G. N., Bjornsson, H., and Arason, P.: The impact of the atmosphere on the Eyjafjallajökull 2010 eruption plume, J. Geophys. Res., 117, D00U07, doi:10.1029/2011JD016762, 2012. 24680

Picquout, A., Lavigne, F., Mei, E., Grancher, D., Noer, C., Vidal, C., and Hadmoko, D.: Air traffic disturbance due to the 2010 Merapi volcano eruption, J. Volcanol. Geoth. Res., 261, 366–375, doi:10.1016/j.jvolgeores.2013.04.005, 2013. 24680

Prata, A. and Bernardo, C.: Retrieval of volcanic SO_2 column abundance from Atmospheric Infrared Sounder data, J. Geophys. Res.-Atmos., 112, D20204, doi:10.1029/2006JD007955, 2007. 24646

Prata, A. J. and Kerkmann, J.: Simultaneous retrieval of volcanic ash and SO_2 using MSG-SEVIRI measurements, Geophys. Res. Lett., 34, L05813, doi:10.1029/2006GL028691, 2007. 24646

Prata, A. J., Carn, S. A., Stohl, A., and Kerkmann, J.: Long range transport and fate of a stratospheric volcanic cloud from Soufrière Hills volcano, Montserrat, Atmos. Chem. Phys., 7, 5093–5103, doi:10.5194/acp-7-5093-2007, 2007. 24680

Prata, A. J., Gangale, G., Clarisse, L., and Karagulian, F.: Ash and sulphur dioxide in the 2008 eruptions of Okmok and Kasatochi: insights from high spectral resolution satellite measurements, J. Geophys. Res., 115, D00L18, doi:10.1029/2009JD013556, 2010. 24679

ACPD
15, 24643–24693, 2015

Pugnaghi, S., Gangale, G., Corradini, S., and Buongiorno, M.: Mt. Etna sulfur dioxide flux monitoring using ASTER-TIR data and atmospheric observations, J. Volcanol. Geoth. Res., 152, 74–90, doi:10.1016/j.jvolgeores.2005.10.004, 2006. 24646

Pumphrey, H. C., Read, W. G., Livesey, N. J., and Yang, K.: Observations of volcanic SO_2 from MLS on Aura, Atmos. Meas. Tech., 8, 195–209, doi:10.5194/amt-8-195-2015, 2015. 24646

Rix, M., Valks, P., Hao, N., Loyola, D. G., Schlager, H., Huntrieser, H. H., Flemming, J., Koehler, U., Schumann, U., and Inness, A.: Volcanic SO_2, BrO and plume height estimations using GOME-2satellite measurementsduring the eruption of Eyjafjallajökull in May 2010, J. Geophys. Res., 117, D00U19, doi:10.1029/2011JD016718, 2012. 24646, 24648, 24653, 24654

Robock, A.: Volcanic eruptions and climate, Rev. Geophys., 38, 191–219, 2000. 24645

Rodgers, C. D.: Inverse Methods for Atmospheric Sounding: Theory and Practice, World Scientific, River Edge, N. J., 2000. 24649

Saepuloh, A., Urai, M., Aisyah, N., Sunarta, Widiwijayanti, C., Subandriyo, and Jousset, P.: Interpretation of ground surface changes prior to the 2010 large eruption of Merapi volcano using ALOS/PALSAR, ASTER TIR and gas emission data, J. Volcanol. Geoth. Res., 261, 130–143, doi:10.1016/j.jvolgeores.2013.05.001, 2013. 24680

Saunders, R. W., Matricardi, M., and Brunel, P.: An improved fast radiative transfer model for assimilation of satellite radiance observations, Q. J. Roy. Meteor. Soc., 125, 1407–1425, doi:10.1002/qj.1999.49712555615, 1999. 24649

Sawamura, P., Vernier, J., Barnes, J., Berkoff, T., Welton, E., Alados-Arboledas, L., Navas-Guzmán, F., Pappalardo, G., Mona, L., Madonna, F., Lange, D., Sicard, M., Godin-Beekmann, S., Payen, G., Wang, Z., Hu, S., Tripathi, S., Cordoba-Jabonero, C., and Hoff, R.: Stratospheric AOD after the 2011 eruption of Nabro volcano measured by lidars over the Northern Hemisphere, Environ. Res. Lett., 7, 034013, doi:10.1088/1748-9326/7/3/034013, 2012. 24662, 24682

Schmidt, A., Carslaw, K. S., Mann, G. W., Rap, A., Pringle, K. J., Spracklen, D. V., Wilson, M., and Forster, P. M.: Importance of tropospheric volcanic aerosol for indirect radiative forcing of climate, Atmos. Chem. Phys., 12, 7321–7339, doi:10.5194/acp-12-7321-2012, 2012. 24644

Schmidt, A., Witham, C. S., Theys, N., Richards, N. A. D., Thordarson, T., Szpek, K., Feng, W., Hort, M. C., Woolley, A. M., Jones, A. R., Redington, A. L., Johnson, B. T., Hayward, C. L., and Carslaw, K. S.: Assessing hazards to aviation from sulfur dioxide emitted by explosive Ice-

ACPD
15, 24643–24693, 2015

landic eruptions, J. Geophys. Res.-Atmos., 119, 14180–14196, doi:10.1002/2014JD022070, 2014. 24645
Scollo, S., Prestifilippo, M., Pecora, E., Corradini, S., Merucci, L., Spata, G., and Coltelli, M.: Eruption column height estimation of the 2011-2013 Etna lava fountains, Ann. Geophys.-Italy, 57, S0214, doi:10.4401/ag-6396, 2014. 24681
Sears, T., Thomas, G., Carboni, E., Smith, A., and Grainger, R.: SO_2 as a possible proxy for volcanic ash in aviation hazard avoidance, J. Geophys. Res.-Atmos., 118, 5698–5709, doi:10.1002/jgrd.50505, 2013. 24645, 24652
Seinfeld, J. H. and Pandis, S. N.: Atmospheric Chemistry and Physics: From Air Pollution to Climate Change, J. Wiley, New York, 1998. 24644
Smets, B., d'Oreye, N., Kervyn, F., Kervyn, M., Albino, F., Arellano, S., Bagalwa, M., Balagizi, C., Carn, S., Darrah, T., Fernandez, J., Galle, B., Gonzalez, P., Head, E., Karume, K., Kavotha, D., Lukaya, F., Mashagiro, N., Mavonga, G., Norman, P., Osodundu, E., Pallero, J., Prieto, J., Samsonov, S., Syauswa, M., Tedesco, D., Tiampo, K., Wauthier, C., and Yalire, M.: Detailed multidisciplinary monitoring reveals pre- and co-eruptive signals at Nyamulagira volcano (North Kivu, Democratic Republic of Congo), B. Volcanol., 76, 1–35, doi:10.1007/s00445-013-0787-1, 2014. 24681
Spinei, E., Carn, S., Krotkov, N., Mount, G., Yang, K., and Krueger, A.: Validation of ozone monitoring instrument SO_2 measurements in the Okmok volcanic cloud over Pullman, WA, July 2008, J. Geophys. Res.-Atmos., 115, D00L08, doi:10.1029/2009JD013492, 2010. 24679
Spinetti, C., Salerno, G., Caltabiano, T., Carboni, E., Clarisse, L., Corradini, S., Grainger, R., Hedelt, P., Koukouli, M., Merucci, L., Siddans, R., Tampellini, L., Theys, N., Valks, P., and Zehner, C.: Volcanic SO_2 by UV-TIR satellite retrievals: validation by using ground-based network at Mt. Etna, Ann. Geophys.-Italy, 57, doi:10.4401/ag-6641, 2014. 24664, 24681
Stevenson, D., Johnson, C., Collins, W., and Derwent, R.: The tropospheric sulphur cycle and the role of volcanic SO_2, Geol. Soc. Sp., 213, 295–305, 2003. 24644
Stevenson, J. A., Loughlin, S., Rae, C., Thordarson, T., Milodowski, A. E., Gilbert, J. S., Harangi, S., Lukács, R., Hojgaard, B., Árting, U., Pyne-O'Donnell, S., MacLeod, A., Whitney, B., and Cassidy, M.: Distal deposition of tephra from the Eyjafjallajökull 2010 summit eruption, J. Geophys. Res., 117, B00C10, doi:10.1029/2011JB008904, 2012. 24680
Stohl, A., Prata, A. J., Eckhardt, S., Clarisse, L., Durant, A., Henne, S., Kristiansen, N. I., Minikin, A., Schumann, U., Seibert, P., Stebel, K., Thomas, H. E., Thorsteinsson, T., Tørseth, K., and Weinzierl, B.: Determination of time- and height-resolved volcanic ash emis-

ACPD
15, 24643–24693, 2015

sions and their use for quantitative ash dispersion modeling: the 2010 Eyjafjallajökull eruption, Atmos. Chem. Phys., 11, 4333–4351, doi:10.5194/acp-11-4333-2011, 2011. 24680
Surono, Jousset, P., Pallister, J., Boichu, M., Buongiorno, M., Budisantoso, A., Costa, F., Andreastuti, S., Prata, F., Schneider, D., Clarisse, L., Humaida, H., Sumarti, S., Bignami, C., Griswold, J., Carn, S., Oppenheimer, C., and Lavigne, F.: The 2010 explosive eruption of Java's Merapi volcano-A "100-year" event, J. Volcanol. Geoth. Res., 241–242, 121–135, doi:10.1016/j.jvolgeores.2012.06.018, 2012. 24680
Textor, C., Graf, H.-F., Herzog, M., and Oberhuber, J.: Injection of gases into the stratosphere by explosive volcanic eruptions, J. Geophys. Res.-Atmos., 108, 4606, doi:10.1029/2002JD002987, 2003. 24645
Theys, N., Van Roozendael, M., Dils, B., Hendrick, F., Hao, N., and De Maziere, M.: First satellite detection of volcanic bromine monoxide emission after the Kasatochi eruption, Geophys. Res. Lett., 36, L03809, doi:10.1029/2008GL036552, 2009. 24680
Theys, N., Campion, R., Clarisse, L., Brenot, H., van Gent, J., Dils, B., Corradini, S., Merucci, L., Coheur, P.-F., Van Roozendael, M., Hurtmans, D., Clerbaux, C., Tait, S., and Ferrucci, F.: Volcanic SO_2 fluxes derived from satellite data: a survey using OMI, GOME-2, IASI and MODIS, Atmos. Chem. Phys., 13, 5945–5968, doi:10.5194/acp-13-5945-2013, 2013. 24659
Theys, N., De Smedt, I., Van Roozendael, M., Froidevaux, L., Clarisse, L., and Hendrick, F.: First satellite detection of volcanic OClO after the eruption of Puyehue-Cordon Caulle, Geophys. Res. Lett., 41, 667–672, doi:10.1002/2013GL058416, 2014. 24682
Thomas, G. E. and Siddans, R.: Development of OCA type processors to volcanic ash detection and retrieval, Final Report, Tech. rep., EUMETSAT RFQ 13/715490, available at: ftp://ftp.rsg.rl.ac.uk/eumetsat_ash/EUMETSAT_RFQ_13-715490_final_report_v2.0.pdf (last access: 8 September 2015), 2015. 24651
Thomas, H. E. and Prata, A. J.: Sulphur dioxide as a volcanic ash proxy during the April–May 2010 eruption of Eyjafjallajökull Volcano, Iceland, Atmos. Chem. Phys., 11, 6871–6880, doi:10.5194/acp-11-6871-2011, 2011. 24652
Tupper, A. and Wunderman, R.: Reducing discrepancies in ground and satellite-observed eruption heights, J. Volcanol. Geoth. Res., 186, 22–31, doi:10.1016/j.jvolgeores.2009.02.015, 2009. 24645
Tupper, A., Textor, C., Herzog, M., Graf, H.-F., and Richards, M.: Tall clouds from small eruptions: the sensitivity of eruption height and fine ash content to tropospheric instability, Nat. Hazards, 51, 375–401, doi:10.1007/s11069-009-9433-9, 2009. 24661

ACPD
15, 24643–24693, 2015

Van Gent, J., Spurr, R., Theys, N., and et al.: Towards operational retrieval of SO_2 plume height from GOME-2 radiance measurements, Atmos. Meas. Tech. Discuss., in preparation, 2015. 24647

Velez, M., Euillades, P., Caselli, A., Blanco, M., and Diaz, J.: Deformation of Copahue volcano: inversion of InSAR data using a genetic algorithm, J. Volcanol. Geoth. Res., 202, 117–126, doi:10.1016/j.jvolgeores.2011.01.012, 2011. 24682

Vernier, J.-P., Thomason, L., Fairlie, T., Minnis, P., Palikonda, R., and Bedka, K.: Comment on "large volcanic aerosol load in the stratosphere linked to Asian monsoon transport", Science, 339, 647d, doi:10.1126/science.1227817, 2013. 24662, 24682

Viccaro, M., Garozzo, I., Cannata, A., Di Grazia, G., and Gresta, S.: Gas burst vs. gas-rich magma recharge: a multidisciplinary study to reveal factors controlling triggering of the recent paroxysmal eruptions at Mt. Etna, J. Volcanol. Geoth. Res., 278–279, 1–13, doi:10.1016/j.jvolgeores.2014.04.001, 2014. 24681

Wadge, G. and Burt, L.: Stress field control of eruption dynamics at a rift volcano: Nyamuragira, D.R. Congo, J. Volcanol. Geoth. Res., 207, 1–15, doi:10.1016/j.jvolgeores.2011.06.012, 2011. 24681

Walker, J. C., Dudhia, A., and Carboni, E.: An effective method for the detection of trace species demonstrated using the MetOp Infrared Atmospheric Sounding Interferometer, Atmos. Meas. Tech., 4, 1567–1580, doi:10.5194/amt-4-1567-2011, 2011. 24649

Walker, J. C., Carboni, E., Dudhia, A., and Grainger, R. G.: Improved detection of sulphur dioxide in volcanic plumes using satellite-based hyperspectral infra-red measurements: application to the Eyjafjallajökull 2010 eruption, J. Geophys. Res., 117, D00U16, doi:10.1029/2011JD016810, 2012. 24647, 24649

Wang, J., Park, S., Zeng, J., Ge, C., Yang, K., Carn, S., Krotkov, N., and Omar, A. H.: Modeling of 2008 Kasatochi volcanic sulfate direct radiative forcing: assimilation of OMI SO_2 plume height data and comparison with MODIS and CALIOP observations, Atmos. Chem. Phys., 13, 1895–1912, doi:10.5194/acp-13-1895-2013, 2013. 24660, 24679

Watson, I., Realmuto, V., Rose, W., Prata, A., Bluth, G., Gu, Y., Bader, C., and Yu, T.: Thermal infrared remote sensing of volcanic emissions using the moderate resolution imaging spectroradiometer, J. Volcanol. Geoth. Res., 135, 75–89, doi:10.1016/j.jvolgeores.2003.12.017, 2004. 24646

ACPD
15, 24643–24693, 2015

Winker, D., Vaughan, M., Omar, A., Hu, Y., Powell, K., Liu, Z., Hunt, W., and Young, S.: Overview of the CALIPSO mission and CALIOP data processing algorithms, J. Atmos. Ocean. Tech., 26, 2310–2323, doi:10.1175/2009JTECHA1281.1, 2009. 24651

Yang, K., Krotkov, N., Krueger, A., Carn, S., Bhartia, P., and Levelt, P.: Improving retrieval of volcanic sulfur dioxide from backscattered UV satellite observations L03102, Geophys. Res. Lett., 36, L03102, doi:10.1029/2008GL036036, 2009. 24646

Yang, K., Liu, X., Bhartia, P., Krotkov, N., Carn, S., Hughes, E., Krueger, A., Spurr, R., and Trahan, S.: Direct retrieval of sulfur dioxide amount and altitude from spaceborne hyperspectral UV measurements: theory and application, J. Geophys. Res.-Atmos., 115, D00L09, doi:10.1029/2010JD013982, 2010. 24646, 24679

Zerefos, C., Ganev, K., Kourtidis, K., Tzortziou, M., Vasaras, A., and Syrakov, E.: On the origin of SO_2 above Northern Greece, Geophys. Res. Lett., 27, 365–368, doi:10.1029/1999GL010799, 2000. 24653

ACPD
15, 24643–24693, 2015

Table 1. Summary of studied eruptions, in chronological order, together with other relevant literature, volcanic explosivity index (VEI) and a short descriptions of the events from the Smithsonian Institution Global Volcanism Programme website (http://www.volcano.si.edu).

Volcano name	Analysed dates	Lat/Lon/ Elevation	Comments on IASI SO_2 plume	References to other work	Volcanic event description (Smithsonian weekly reports)
Llaima (Chile)	2–6 Jan 2008	38.692° S 71.729° W 3125 m	Small eruption (maximum of 0.04 Tg of SO_2). Plume connected to the volcano only on the first day. Confined in troposphere.	McCormick et al. (2013): OMI SO_2 study.	VEI 3. Strombolian eruption began 1 Jan; ash plumes to 12.5 km on 2 Jan, and to 3.7 km on 3 Jan.
Okmok (Aleutian islands)	12–20 Jul 2008	53.43° N 168.13° W 1073 m	SO_2 injected around tropopause and the plume spreads south (pacific ocean) and east (north America) from the volcano. Presence of intermittent smaller and lower plume connected with the volcano. Main plume altitude increases with time following the tropopause altitude.	Spinei et al. (2010): OMI SO_2 validation against ground measurements over north America; Prata et al. (2010): SO_2 and ash from AIRS.	VEI 4. Strong explosive eruption began 12 Jul, with ash to at least 15 km. Eruption intensity declined, with ash plumes to 6 km on 17 Jul. Eruptions on 19 Jul sent ash to 9 km.
Kasatochi (Aleutian islands)	7–22 Aug 2008	52.177° N 175.508° W 314 m	SO_2 amount reached the maximum after seven days indicating continuous injection from volcano. Within ten days SO_2 plume affected all latitudes between 30–90° N. Reached to tropopause and stratosphere.	Krotkov et al. (2010): Dispersion and lifetime of the SO_2 using OMI; Yang et al. (2010): OMI retrieval of SO_2 amount and altitude; Karagulian et al. (2010): SO_2 and ash from IASI; Corradini et al. (2010): Comparison of different IR instruments (AIRS, MODIS); Kristiansen et al. (2010): inverse transport modelling; Bitar et al. (2010): lidar measurements, injected material into the troposphere and lower stratosphere; Prata et al. (2010): SO_2 and ash from AIRS; Nowlan et al. (2011): GOME-2 optimal estimation retrieval of amount and altitude; Wang et al. (2013): Volcanic sulfate forcing uning OMI SO_2.	VEI 4. Explosive eruption began on 7 Aug, with ash plumes to 14 km; continuous eruptions from 8–9 Aug, with ash plumes to 9–14 km. Subsequent observations obscured by cloud.
Alu-Dalaffilla (Ethiopia)	4–7 Nov 2008	13.792° N 40.55° E 613 m	Plume is divided in two parts from the beginning (one lower in troposphere and one higher into tropopause /stratosphere). SO_2 near the volcano in every image (continuous emission). Nearly one order of magnitude smaller than Nabro (in amount of SO_2) but reached comparable height.	Pagli et al. (2012): Ethiopian Rift deformation paper, studying the source of Alu-Dalafilla Eruption. Mallik et al. (2013): Enhanced SO_2 concentrations observed over northern India in Nov 2008.	VEI 3 – Mainly effusive eruption. Strong fissure eruption began on 3 Nov, for a few hours, waned rapidly and ended on 6 Nov. (Pagli et al., 2012). No direct observations of the eruption.

ACPD
15, 24643–24693, 2015

Table 1. Continued.

Volcano name	Analysed dates	Lat/Lon/ Elevation	Comments on IASI SO_2 plume	References to other work	Volcanic event description (Smithsonian weekly reports)
Sarychev Peak (Kuril islands)	11–26 Jun 2009	48.092° N 153.2° E 1496 m	Started with a small tropospheric plume building up with increasing SO_2 load, maximum on 16 Jun (0.6 Tg). Reached tropopause and stratosphere.	Theys et al. (2009): Volcanic BrO from GOME-2. Haywood et al. (2010): Climate model (HadGEM2), IASI SO_2, OSIRIS limb sounder and CALIPSO lidar measurements to investigate the distributions of SO_2 and radiative impact of sulphate aerosol; Carn and Lopez (2011): validation of OMI SO_2; Doeringer et al. (2012): sulphate aerosols and SO_2 from the Atmospheric Chemistry Experiment (ACE) measurements; Fromm et al. (2014); on correction for OSIRIS dataset and using SO_2 from C12.	VEI 4. Eruption began 11 Jun, with ash plumes to 7.5 km on 12 Jun, and a strong ash plume to 12 km on 14 Jun. Further explosions with ash to 10–14 km continued through 18 Jun.
Soufrière Hills (Montserrat)	10–15 Feb 2010	16.72° N 62.18° W 915 m	When it was first observed the SO_2 plume is divided into two parts: a higher one around 16–19 km (tropopause/stratosphere) and a lower one in the troposphere. The lower plume disappeared (non detectable) after one day, while the higher one spread east, south east.	Prata et al. (2007) on 2006 eruption. Carn and Prata (2010): satellite measurements for 1995–2009; Christopher et al. (2010) include SO_2 measurments for 1995–2009. Wadge 2010: Lava production for the period 1995–2009. Christopher et al. (2014): SO_2 degassing, for 1995– 2013, and relation with magma supply; Nicholson et al. (2013), include daily mean SO_2 flux.	VEI 3. Large dome collapse on 11 Feb, with pyroclastic flows and an ash plume to 15 km.
Eyjafjallajökull (Iceland)	14 Apr–24 May 2010	63.63° N 19.62° W 1666 m	SO_2 plume confined in troposphere. Up to 20 Apr the plume was below 10 km (mainly confined within 5 km); From 20 to 30 Apr plume < 5 km. Increase in both (amount and altitude) from 5 May, with maximum altitude (around 10 km) from 14 to 17 May.	Stohl et al. (2011): ash emission height from inversion with dispersion model FLEXPART. Marzano et al. (2011): radar measurements of plume altitude. Stevenson et al. (2012): tephra deposit. Petersen et al. (2012): impact in atmosphere and plume altitude. Carboni et al. (2012): IASI SO_2. Boichu et al. (2013): chemistry-transport model + IASI SO_2 to invert SO_2 flux.	VEI 4. Explosive eruptions from the summit, with ash plumes from 3–10 km (Gudmundsson et al., 2012).
Merapi (Java, Indonesia)	4–11 Nov 2010	7.542° S 110.442° E 2968 m	High plume up to tropopause and stratosphere. (Problems: old plume overpassing the volcano).	Surono et al. (2012): estimate a total of 0.44 Tg of SO_2, using IASI -AIRS assuming a plume altitude of 16 km. Saepuloh et al. (2013); Picquout et al. (2013); Pallister et al. (2013); Luehr et al. (2013); Jenkins et al. (2013); Innocenti et al. (2013b, a); Cronin et al. (2013); Costa et al. (2013); Budi-Santoso et al. (2013)	VEI 4. Major explosive eruption, with a climactic phase that began on 3 Nov with ash plumes to 18 km. Strong explosions continued through 5–6 Nov (17 km ash plumes), declining to < 8 km by 12 Nov.

ACPD
15, 24643–24693, 2015

Table 1. Continued.

Volcano name	Analysed dates	Lat/Lon/ Elevation	Comments on IASI SO_2 plume	References to other work	Volcanic event description (Smithsonian weekly reports)
Etna (Sicily, Italy)	23–25 Nov 2007 + 2011 fountains	37.734° N 15.004° E 3330 m	All episodes considered are confined to the troposphere.	Aiuppa et al. (2010); combine seismic (volcanic tremor and long-period seismicity), deformation (GPS), and geochemical (volcanic gas plume CO_2/SO_2 ratios) measurements to interpret trends in the recent (2007–2008) activity of Etna volcano. Patane et al. (2013); study the 2011 Etna episodes using multi-parameter approach (sesmicity, ground deformations and geochemistry, SO_2 flux, CO_2 flux, CO_2/SO_2 ratio). Viccaro et al. (2014); Behncke et al. (2014); Birth, growth and products of the new SE crater. Scollo et al. (2014); Eruption column height estimation (using calibrated TIR camera) of the 2011–2013 Etna lava fountains. Guerrieri et al. (2015): ash and SO_2, retrieval and flux estimate, from SEVIRI. Spinetti et al. (2014), satellite SO_2 validation with ground measurements (including this IASI SO_2 scheme).	
Nyamuragira/ Nyiragongo (DR Congo)	3–12 Jan 2010 and 7–15 Nov 2011	1.408° S 29.2° E 3058 m/ 1.52° S 29.25° E 3470 m	Confined to the troposphere.	Carn and Bluth (2003); Nyamuragira SO_2 from TOMS period: 1978–2002. Bluth and Carn (2008); Exceptional sulphur degassing from Nyamuragira volcano using TOMS, 1979–2005. Wadge and Burt (2011). Carn et al. (2013): monitored Nyiragongo volcano degassing with OMI, including monthly means SO_2 for 2004–2008. Cuoco et al. (2013): impact of Nyamuragira. Campion (2014): studied Nyamuragira emissions of SO_2 using OMI and ASTER. Smets et al. (2014): multidisciplinary monitoring reveals pre- and co-eruptive signals at Nyamuragira volcano associated with the Jan 2010 volcanic eruption (seismic and OMI data).	Jan 2010, VEI 1. (Nyamuragira). A flank fissure eruption began on 2 Jan 2010, and continued intermittently for 3–4 weeks. Nov 2011, VEI 2. (Nyamuragira): major flank fissure eruption began with fire-fountaining and the emplacement of a long lava flow on 6 Nov 2011. The eruption is thought to have ceased by 18 Nov. During both Jan 2010 and Nov 2011, the lava lake at Nyiragongo remained active (based on thermal alerts).

ACPD
15, 24643–24693, 2015

Table 1. Continued.

Volcano name	Analysed dates	Lat/Lon/ Elevation	Comments on IASI SO_2 plume	References to other work	Volcanic event description (Smithsonian weekly reports)
Grímsvötn	21–26 May 2011	64.42° N 17.33° W 1725 m	Higher part of the plume moved west and spread north reaching the tropopause/stratosphere. Lower plume travelled towards Europe (together with ash), confined to the troposphere.	Flemming and Inness (2013): Assimilation of UV satellite measurements for forecast. Moxnes et al. (2014): FLEXPART + IASI SO_2 and ash. Koukouli et al. (2014): Intercomparison of SO_2 from IASI (including C12), GOME-2 and ground data.	VEI 4. Strong explosive eruption, with an ash plume to 20 km on 21 May, declining to 10–15 km on the morning of 22 May. Minor activity on 24 May, with ash to 5–7 km.
Puyehue-Cordon-Caulle	5–30 Jun 2011	40.59° S 72.117° W 2236 m	Intermediate magnitude (between Llaima and Copahue) Reached the tropopause/stratosphere and we can follow the plume going 3 times around the Southern Hemisphere in 30 days. First part of the eruption is higher in SO_2 amount and altitude. Intermittent low plume connected with the volcano for all the period considered.	Theys et al. (2014): detection of volcanic OClO. Bignami et al. (2014): SAR deformation, MODIS ash and SO_2.	VEI 5. Major sequence of explosive and effusive eruptions, that began on 4 Jun with ash plumes to 11–14 km. For the rest of Jun, lower-level eruptive activity persisted, with intermittent ash plumes to 5–8 km. The eruption continued until Apr 2012.
Nabro	12–23 Jun 2011	13.37° N 41.7° E 2218 m	The highest emission of SO_2 for the period considered (2008–2012). Two plumes at different altitudes, the highest one reached the to stratosphere, the lower remained confined to the troposphere.	Fromm et al. (2014): Nabro injected sulphur directly to or above the tropopause upon the initial eruption on 12/13 Jun, and again on 16 Jun 2011. Bourassa et al. (2012); Sawamura et al. (2012); Vernier et al. (2013); Fromm et al. (2013); Bourassa et al. (2013); Clarisse et al. (2014); Biondi et al. (2015).	VEI 4. The eruption began with a major ash plume, to 9–14 km on 12 Jun. The activity continue dominated by lava flow, and with ash plumes to 6–8 km from 15–19 Jun.
Copahue	22–27 Dec 2012	37.856° S 71.183° W 2953 m	Maximum of 0.72 Tg of SO_2 present in atmosphere. Plume connected with volcano every day. Confined to the troposphere.	Velez et al. (2011): ground deformation using InSAR; Bonali (2013): earthquake and stress study.	VEI 2. Moderate explosive eruptions, with a mixture of Strombolian fire-fountaining and steam-driven phreatic explosions, producing frequent low-level ash plumes rising 1–2 km above the crater rim.

ACPD
15, 24643–24693, 2015

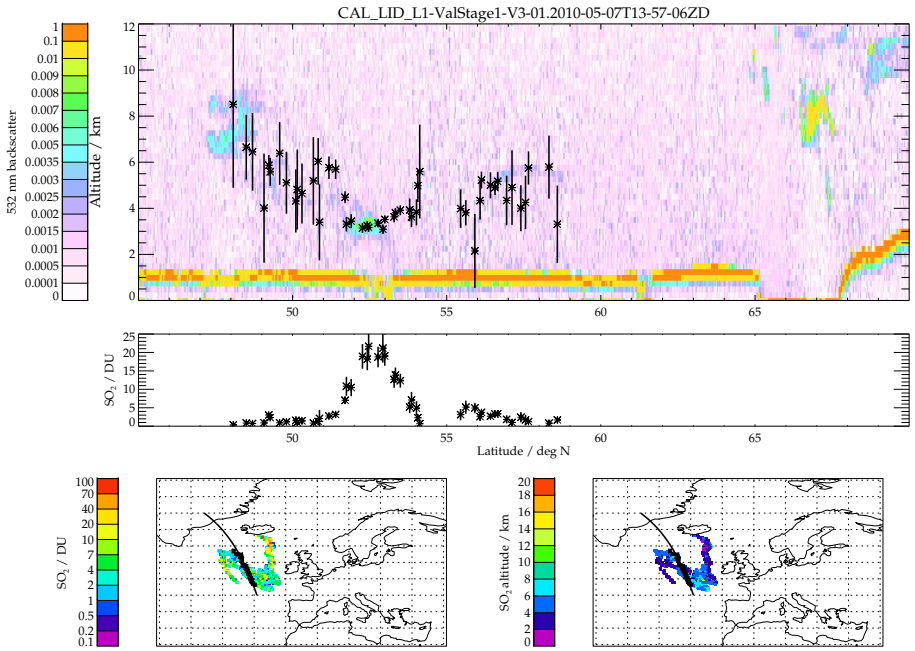

Figure 1. CALIOP/ IASI coincidences for the Eyjafjallajökull plume on 7 May 2010 overpasses within 2 h off each other. Top plot: CALIOP backscatter profile with IASI over-plotted retrieval altitude (black stars) and error-bar (black line); middle plot: the IASI SO_2 amount and error-bars corresponding to the altitude plotted above; bottom plots: map of IASI SO_2 amount (left) and altitude (right) with CALIPSO track (black line) and identifying the IASI pixel plotted above with black stars.

ACPD
15, 24643–24693, 2015

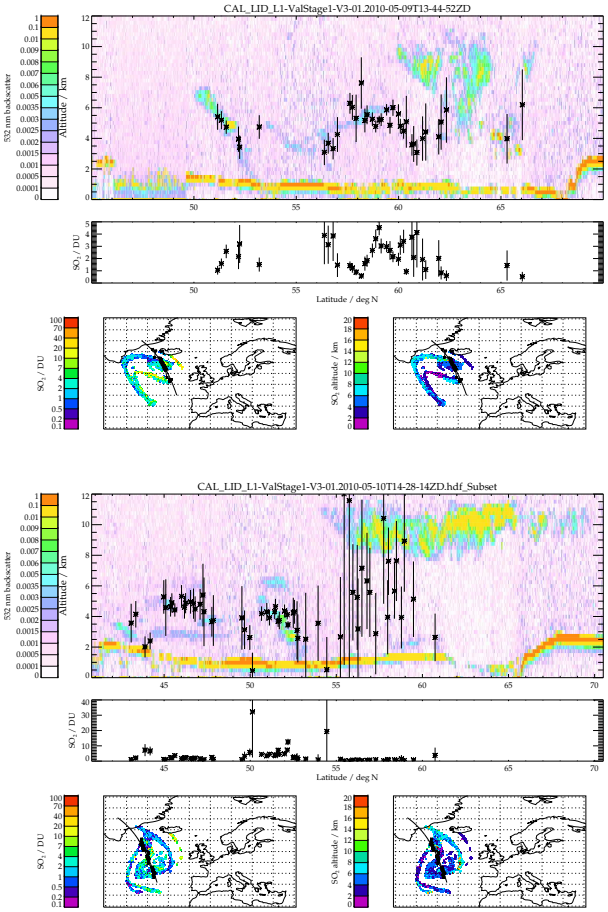

Figure 2. CALIOP-IASI coincidences for the 9 and 10 May 2010, Eyjafjallajökull plume. As Fig. 1.

ACPD
15, 24643–24693, 2015

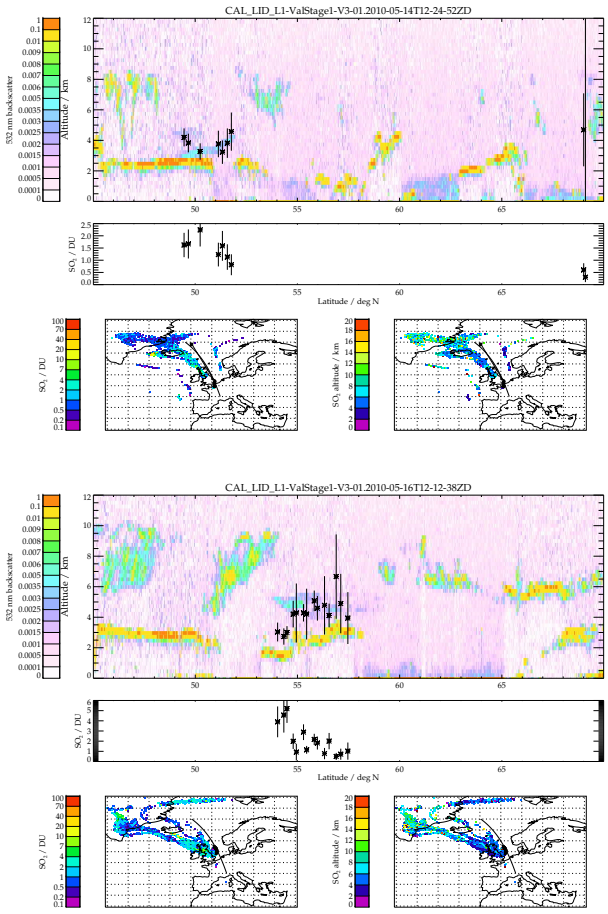

Figure 3. CALIOP-IASI coincidences for the 14 and 16 May 2010, Eyjafjallajökull plume. As Fig. 1.

ACPD
15, 24643–24693, 2015

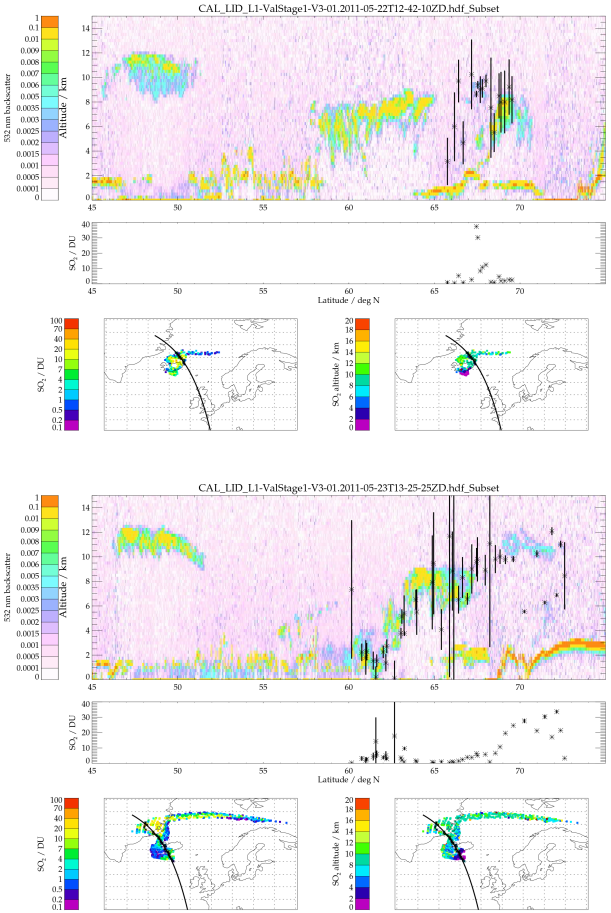

Figure 4. CALIOP/IASI coincidences for the Grímsvötn eruption on 22 and 23 May 2011. As Fig. 1.

ACPD
15, 24643–24693, 2015

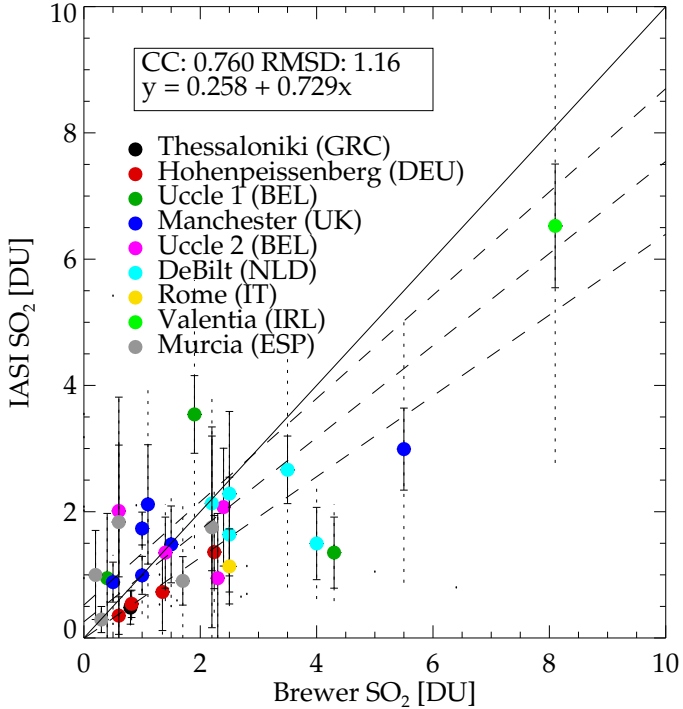

Figure 5. Scatter plot of IASI SO_2 measurements, averaged within a distance of 200 km from the ground station, vs. the daily SO_2 column amount, measured from Brewer spectrometers. Different colours correspond to a different Brewer ground station. Black error-bars are the IASI average errors; dotted error-bars are the standard deviation of the IASI data within the selected distance. Black lines represent the ideal line $y = x$; dotted lines are the best fits with error in the best fit. The legend box shows the correlation coefficient (CC), root mean square difference (RMSD) and the best fit line.

ACPD
15, 24643–24693, 2015

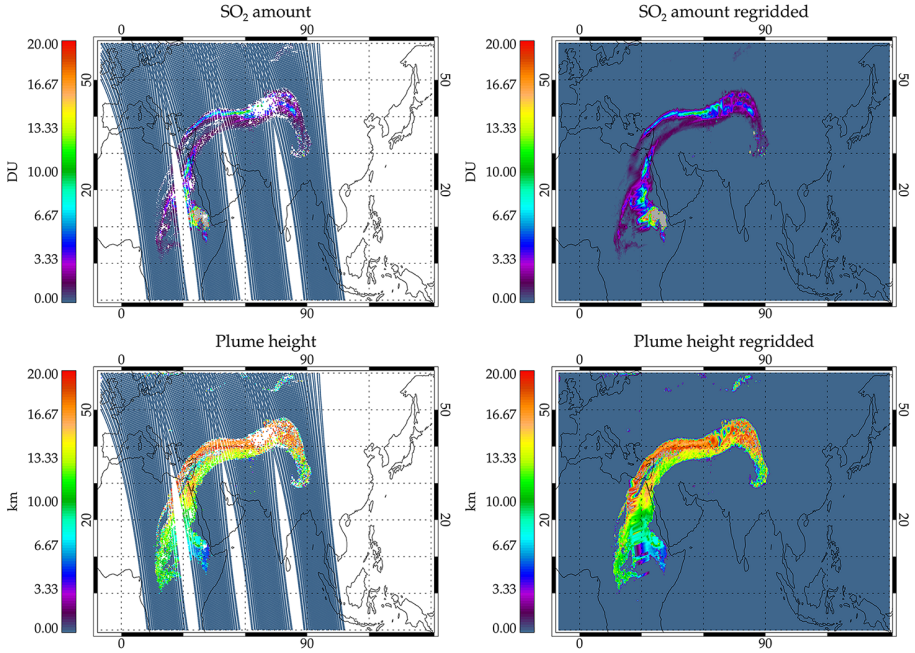

Figure 6. Maps of IASI SO_2 amount (top left) and height (bottom left) and the equivalent maps of SO_2 amount (top right) and height (bottom right) obtained after regridding. The IASI data are a combination of four orbits on the 15 June 2011 from 13:00 to 18:00 UTC.

ACPD
15, 24643–24693, 2015

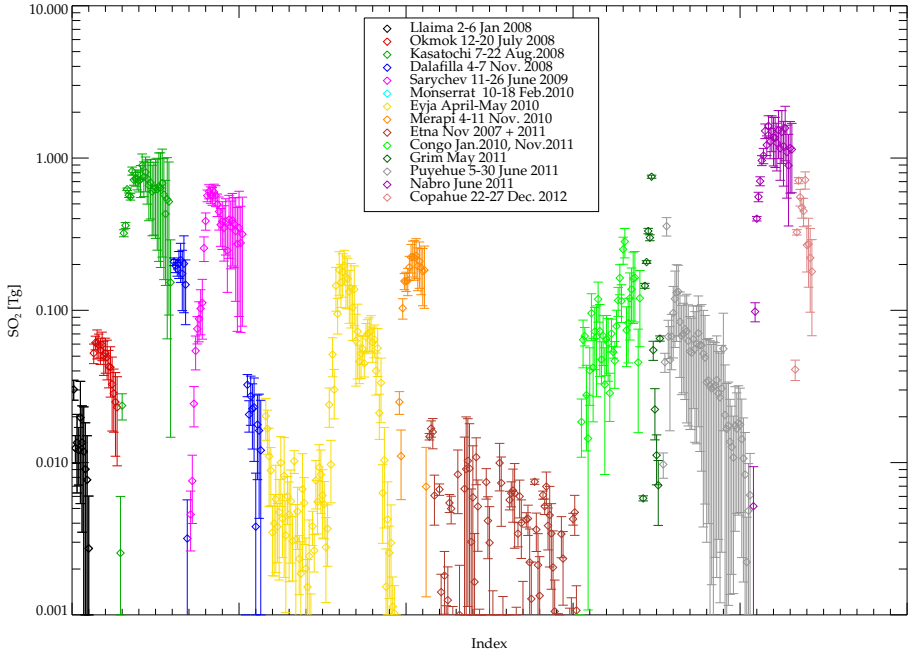

Figure 7. SO_2 mass present in the atmosphere as retrieved from IASI data. The values are the measured amount every half day and vary with volcanic emission, gas removal and satellite sampling. Points are separated by ~ 12 h. Data are presented in temporal order along the ordinate (x axis) but eruptions are plotted consecutively one after the other without a gap between them.

ACPD
15, 24643–24693, 2015

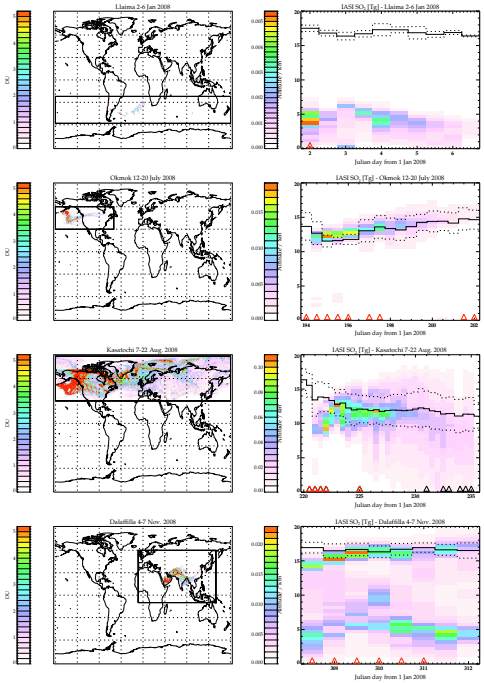

Figure 8. The left column shows the plots of the maximum SO_2 amount retrieved within the considered area (black rectangle). The right column shows the SO_2 vertical distribution for the considered volcanic eruption. In each plot the *y* axes are the vertical levels in km. The colour represents the total mass of SO_2 in Tg, dark-red represents values higher than the colour-bar. Every column of the plots come from an IASI map (one every 12 h). Red triangles in the bottom line indicate the presence of a fresh plume connected with the volcano, black triangles indicate the presence of an old plume overpassing the volcano (this may eventually mask a newer plume). Note that the plots for different eruptions have different colour-scales and cover different time ranges.

ACPD
15, 24643–24693, 2015

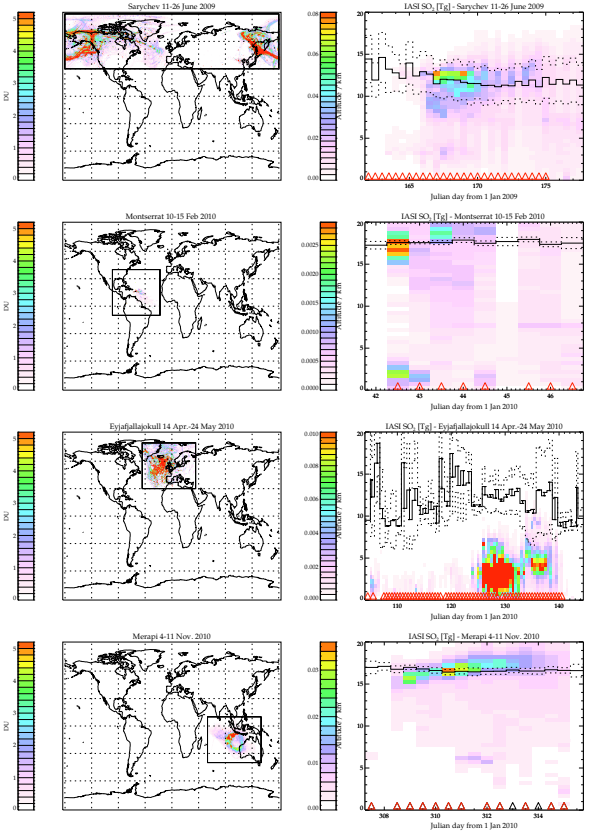

Figure 9. As for Fig. 8.

ACPD
15, 24643–24693, 2015

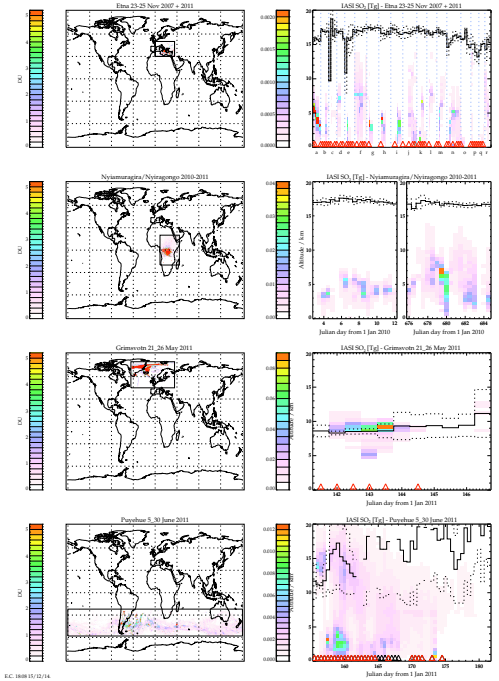

Figure 10. As for Fig. 8. The Etna plots shows different eruptive episodes corresponding to *x* axes labels: (a) 23–25 November 2007 eruption; and the 2011 lava-fountains: (b) 11–13 January, (c) 17–19 February, (d) 10–12 April, (e) 11–13 May, (f) 8–10 July, (g) 18–20 July, (h) 24–26 July, (i) 29 July–1 August, (j) 4–7 August, (k) 11–13 August, (l) 19–21 August, (m) 28–30 August, (n) 7–10 September, (o) 18–20 September, (p) 28–30 September, (q) 11–14 October, (r) 12–17 November.

ACPD
15, 24643–24693, 2015

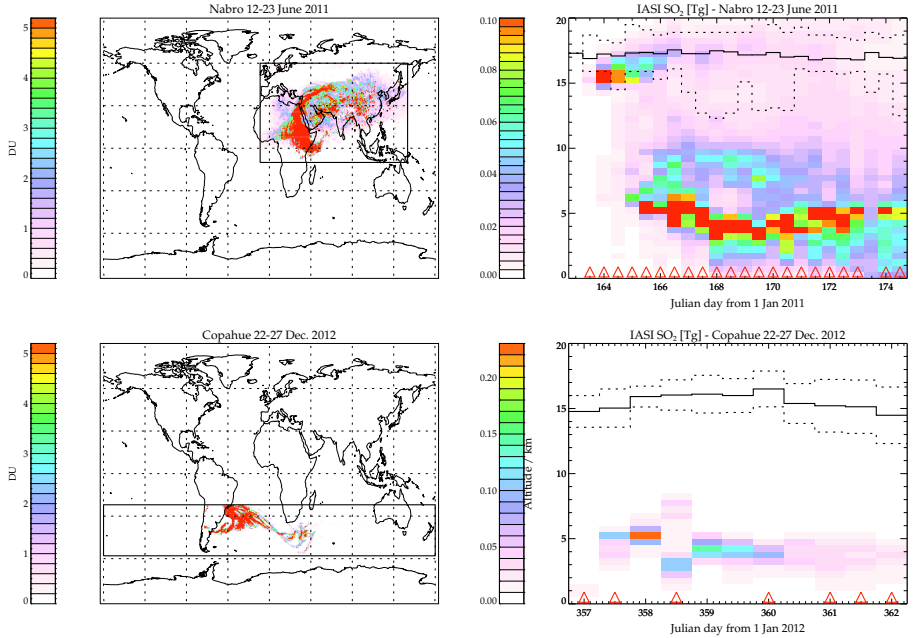

Figure 11. As for Fig. 8.

ACPD
15, 24643–24693, 2015